Mathematical Analysis on the PEC model for Thixotropic Fluids

Taige Wang

Dissertation submitted to the Faculty of the
Virginia Polytechnic Institute and State University
in partial fulfillment of the requirements for the degree of

Doctor of Philosophy
in
Mathematics

Prof. Michael Renardy, Chair
Yuriko Renardy
Robert Rogers
Shu-Ming Sun

March 22, 2016
Blacksburg, Virginia

Keywords: Complex Fluids, Thixotropy, Multiscales, Shear Banding

Mathematical Analysis on the PEC model for Thixotropic Fluids

Taige Wang

(ABSTRACT)

A lot of fluids are more complex than water: polymers, paints, gels, ketchup etc., because of big particles and their complicated microstructures, for instance, molecule entanglement. Due to this structure complexity, some material can display that it is still in yielded state when the imposed stress is released. This is referred to as thixotropy. This dissertation establishes mathematical analysis on a thixotropic yield stress fluid using a viscoelastic model under the limit that the ratio of retardation time versus relaxation time approaches zero. The differential equation model (the PEC model) describing the evolution of the conformation tensor is analyzed. We model the flow when simple shearing is imposed by prescribing a total stress.

One part of this dissertation focuses on oscillatory shear stresses. In shear flow, different fluid states corresponding to yielded and unyielded phases occur. We use asymptotic analysis to study transition between these phases when slow oscillatory shearing is set up. Simulations will be used to illustrate and supplement the analysis.

Another part of the dissertation focuses on planar Poiseuille flow. Since the flow is spatially inhomogeneous in this situation, shear bands are observed. The flow is driven by a homogeneous pressure gradient, leading to a variation of stress in the cross-stream direction. In this setting, the flow would yield in different time scales during the evolution. Formulas linking the yield locations, transition width, and yield time are obtained. When we introduce Korteweg stress in the transition, the yield location is shifted. An equal area rule is identified to fit the shifted locations.

Key Points: Thixotropy, Regime, Oscillatory Shearing, Steady Shearing, Shear Band, Korteweg Stress

Contents

List of Figures

List of Tables

Chapter 1

Introduction

1.1 Yield stress fluids and thixotropic fluids

A broad variety of fluids is seen in nature: water, oil, alcohol, paste, colloids, suspensions, etc. Among them, many fluids categorized as complex fluids such as pastes and colloids show a yield stress phenomenon, i.e. they will flow only when the applied stress is over a critical value (yield point). Well-known "traditional" theory of yield stress fluids has been established by generalized Newtonian models such as the Bingham or Herschel-Bulkley fluid. The yield point is clearly defined in such models. We cite two review papers [6, 38] for reviews on yield stress fluids.

However, a lot of yield stress fluids display thixotropy in experiments. That is, the structure breaks down when the stress is imposed and builds up when the stress is absent. This phenomenon is not captured by Bingham models. The time-scales of physical interest can range up to several hours in microstructure buildup. Many yield stress fluids are thixotropic. That is they remain yielded long after the motion has ceased.

Thixotropy is a challenge to analyze owing to the fact that the microstructure change is complex, and presently there is no good model capturing this complexity. However, this phenomena is as common as Bingham fluids in nature and industry since many yield stress fluids have thixotropy. For instance, it can be seen in processing of cosmetics, food science and using chemical products like paints, gels, or muds. A typical example of thixotropy is when you want some ketchup: you might knock the bottom, shake the bottle or put the bottle up-side-down while the ketchup flows slowly. Once ketchup flows out anyway and you leave the bottle standing as it was, it won't take much effort to get more the second time. You also may observe that when the ketchup flows out of the bottle, the rest will flow out quickly. This observation is referred to as the memory of fluid which is that the fluid "memorizes" the history of yielding and won't take a long time to yield again.

Other challenges are present such as stress overshoots (see e.g. [38]) and hysteresis (i.e. fluids "unyield" at a much lower stress than the yield point in [14, 27]) which are also common and hard to describe theoretically as well can occur for yield stress fluids. These phenomena cause coexistence of yielded and unyielded phases at the same stress and shear banding (see e.g. [36]). Moreover, the critical value of yield stress may depend on the observation time in experiments; "slow" yielding occurs at lower values of stress than "fast" yielding in [12, 11, 50] (fluid yields after long time when no flow is observed). These phenomena lead to considerable ambiguity in defining "yield stress". A yield stress defined by traditional models such as Bingham model may in fact hide more complex dynamics over unresolved time scales (see [4]). Based on this reasoning, there is no "true" yield stress in many cases.

In the next section, we briefly track the concept of thixotropy and the usual ways on how to portray it.

1.2 The term: thixotropy

As reviewed in [5], thixotropy as a phase-change phenomenon was found by Schalek and Szegvari in 1923, who noted that "gels have the remarkable property of becoming completely liquid through gentle shaking alone, to such an extent that the liquified gel is hardly distinguishable from the original sol. These sols were liquified by shaking, solidified again after a period of time". This was the first description of the thixotropy phenomenon and later was recorded in Peterfi's paper [40]. The word "thixotropy" is made by combining "thixis" (stirring or shaking) and "trepo" (changing or turning). The first special book on thixotropy by Freundlich is "Thixotropie" ([23]) on introduction of isothermal fluid properties of aluminum hydroxide gels. This earliest use of the term is for the reversible transition from fluid to elastic gel. During the later decades, different meanings were thrust into this definition.

As more thixotropic fluids and phenomena were found, probed, and investigated, thixotropy was used to indicate the reduction of viscosity which happens reversibly with time dependence on applied shearing. Sometimes "thixotropy" refers to time dependence of yield stress in flows or flow history to non-linear behavior ([12]). These ideas then form two points of view. One emphasizes the transitions in molecular structure, e.g. between gel and liquid. The gel state disappears when shaking it while appears again on standing. A lot of materials like adhesives, coatings, paints are known to have this property. The second emphasizes time dependence of rheological properties like viscosity (see Pryce-Jones [42]). This type of behavior differs from simple shear thinning as it is common in polymers by the long time persistence of reduction in viscosity after cessation of shearing.

A lot of definitions can be found in the literature. Here we cite some paragraphs of [5] discussing different thixotropy definitions:

> In J. Thewlis (Ed.), Oxford Encyclopedia Dictionary of Physics, Pergamon Press, Oxford, 1962: "Certain materials behave as solids under very small applied stresses but under greater stresses become liquids. When the stresses are removed the material settles back into its original consistency."
>
> In T.C. Collocott (Ed.), Chambers Dictionary of Science and Technology, W & R Chambers, Edinburgh, 1971: "Rheological property of fluids and plastic solids characterized by a high viscosity at low stress, but a decreased viscosity when an increased stress is applied."
>
> In D.M. Considine (Ed.), Van Nostrand's Scientific Encyclopedia, 5th. end., Van Nostrand Reinhold Company, New York, 1976: "A thixotropic fluid is a fluid whose viscosity is a function not only of the shearing stress, but also of the previous history of motion within the fluid. The viscosity usually decreases with the length of time the fluid has been in motion."
>
> In T. Whelan (Ed.), Polymer Technology Dictionary, Chapmen & Hall, London, 1994: "A term used in rheology which means that the viscosity of a material decreases significantly with the time of shearing and then, increases significantly when the force inducing the flow is removed."
>
> In Chambers 20th Century Dictionary, Chambers, London, 1993: "Thixotropy: the property of gels of showing a temporary reduction in viscosity when shaken or stirred."

These definitions summarize thixotropy from different aspects as the consequence of a cycle of transitions from solid-like to liquid-like under shearing and recovery when the shearing is released (reversibility). Time effects on phase, deformation, viscosity, etc. are also identified as important aspects of thixotropy. Moreover, thixotropy implies "shear thinning" since the solid-like state at rest has high viscosity while the liquid state under stress has much lower viscosity. We interpret thixotropy as the long persistence of a yielded state even after the fluid returns to rest.

1.3 Thixotropic phenomena

Materials with internal microstructure can display thixotropy as long as the phase transitions are caused by the reformulation of microstructure from one state to another and recovery during shearing-resting. Microstructure change is caused by the competition and balance of breakdown and buildup. When a shearing is imposed, the flow stress tears the microstructure (breakdown) while buildup is present as particle collisions and their Brownian motions. The Brownian motion is referred to as the thermal agitation by atoms and molecules pushing particles to move to new positions, which are easy to form a microstructure via attracting each other. Microstructure refers to spatial distribution of particles, arrangement of fibers

and entanglement density etc. These changes in micro level determine viscosity, elasticity, phase, and other rheological properties of the fluid.

Because the molecules are big with complex microstructure such as entanglement bringing great and complex viscous response, it can take an extremely long time to test materials or observe reasonable deformation. These time scales are often longer than the response time of equipment, the flow time and even the experimenter's expected waiting time in patience. It might be that the breakdown time of microstructure would be on the scale of seconds while the buildup time is days. In spite of this, time scales are significant not only to evaluate thixotropy, but also a cumulative effect from the flow history on the flow. Time dependency and memory in viscoelasticity are used to understand thixotropy. It will be clear that thixotropy can be analyzed using similar models as done for viscoelasticity.

As a caveat, we note that thixotropy can also be modeled as distinct from viscoelasticity. This difference appears in inelastic thixotropy ([34]), which can be combined with viscoelasticity and produces different time scales when they interplay ([8]).

As we see from all the above paragraphs, thixotropy is a complicated phenomenon, which attracts interest from experimental researchers. Here are several general ways of imposing shear rate or stress to look at response of materials for testing (see [34, 8]):

1. Loop test (Hysteresis)

   In this experiment, the experimenter increases the shear rate from 0 continuously to the maximum then decreases to 0. If the flow curve by transient data forms a hysteresis loop, the material is suggested to be thixotropic. The areas enclosed by the loop are different for different materials. It is related to the flow history and used to evaluate thixotropy. Although this area is influenced by other conditions such as the rate of change of shearing, this test is a clear means to show thixotropy. There are some cons in loop tests. For instance, the curve shape obtained might be influenced for the same material if slower application of shear rate causes different change of microstructure. It is often hard to tell the effect of two parameters: time and shear rate in the experiment, which can be avoided by the step-wise change in shear rate.

2. Step-wise changes of shear rate or shear stress (Step experiments)

   For step-wise change of shear rate, the shearing has constant rate to produce a steady state. The key is then to stepping-up or down the rate to probe the response of the material. Viscosity is observed to have abrupt change as the response of microstructure. Moreover, the reversibility is produced if applying the reverse stepping process at this time. It has advantage over the loop test since the shear rate effect is isolated from other factors. By applying step change of stress, yield stress is displayed in that the viscosity change is sensitive to different step stress as a bifurcation picture.

3. Start-up and creep test

A start-up constant shearing is suddenly applied on the material which has been at rest for some time. Stress overshoot is observed first and then stress decreases to steady state. The thixotropic recovery is displayed by the plot of overshoot stress vs rest time. Creep test is the means that a constant stress is invoked to get strain as a function of time in plots. Yield stress behavior is displayed in this test as well. The shearing history is observed to be related to the yield stress value. The shear rate decreases and surges up again after delay when applying constant stress. This delay shrinks when the stress is increased.

4. Large Amplitude Oscillatory Shear (LAOS)

   Recently oscillatory shearings as transient and nonlinear test are invoked for probing thixotropy (see [17, 8, 56]). Compared to instantaneous step-wise change, oscillatory stress or strain input is easier to set in the equipment. The measurement of responses are more precise as well owing to the regular oscillations of input and output. It also provides more convenient analysis since the response is decomposed into harmonic series or viscous and elastic parts. A great length of this dissertation will handle the fluid response under LAOS stress.

For the need of analysis, the constitutive models are postulated. In the next section, we'll go over previous constitutive models and present the very model we are interested in.

1.4 Theoretical models: Generalized Newtonian fluid, structure parameter, viscoelasticity

We already have seen what are effective ingredients for thixotropy and how to recognize and evaluate them. In this section, we will review the earlier efforts for understanding wider categories of yield stress fluids. There are many models involving different theories already and we just cover categories which are typical, related, or potentially useful to our work.

The earliest model posed for complex fluids is the Bingham or Herschel-Bulkley model. In these models, the yield stress behavior is "built" in the model as a yield point is added into the Newtonian fluid model as the following constitutive equation:

$$\tau = \tau_0 + \eta\dot{\gamma}. \tag{1.1}$$

τ is the stress, η is the viscosity of fluid and $\dot{\gamma}$ is the deformation rate. This equation depicts the material which behaves like solid when the imposed force is less than the critical yield stress τ_0; on the other hand, the material behaves like liquid if the force is over τ_0. This

model is the earliest effort from models modified from Newtonian fluid to fit the yield stress behavior of complex fluids hence classified as generalized Newtonian fluids.

In the simplest case, η is a constant for given temperature, pressure, composition, density of fluid, etc. However, the situation would be more complicated if the viscosity is variable: for instance, η can be a constant multiple of power of deformation rate: $m\dot{\gamma}^{n-1}$. In this manner, the constitutive relation (1.1) becomes a power law. This variable viscosity can be built into existent models, for example, the Navier-Stokes equations.

Further efforts have been made in the past decades to understand complex fluids within a different context than generalized Newtonian models. Typically, these "new" theories add a structure parameter to relatively "simple" yield stress fluids such as the Bingham or Herschel-Bulkley models. This parameter doesn't need to be deformation rate and does measure the change or deformation of microstructure. The viscosity ([39]) or the power law exponent ([22]) can depend on this structure parameter.

This parameter is sometimes denoted as λ and it has its own kinetic model, which is coupled with the constitutive equations of stress. One such model for instance combining power laws reads:

$$\frac{d}{dt}\lambda = a(1-\lambda)^b - c\lambda\dot{\gamma}^d.$$

This model is identified as a two-process model in [5] to illustrate indirect microstructure theories. As the key in this kind of theory, λ takes values on $[0, 1]$. $\lambda = 1$ stands for that microstructure has built up whereas $\lambda = 0$ stands for microstructure breakdown. This model easily portrays the competition and coexistence of buildup and breakdown. Usually during this deformation process, the viscosity also changes, say, from η_0 to η_∞ if the structure from initial rest is deformed due to flow. A similar model is also employed in [8] to predict LAOS effects on cycles of breakdown and buildup.

As another modeling strategy, such analysis can be done by looking at viscoelastic models revised by adding structure parameters. There are a number of differential models for stress tensor in viscoelasticity. The elementary ones are the Maxwell and Jeffrey models for linear viscoelasticity. The basic idea is to combine the stress from viscous contribution of Newtonian and elastic contribution of Hookean effects (see [7]). Maxwell writes up the constitutive equation for simple shearing flow as

$$T_{12} + \frac{\eta}{G}\frac{\partial}{\partial t}T_{12} = \eta\dot{\gamma}$$

with modulus G and T_{12} is 1-2 entry of stress tensor $\mathbf{T}$. It could be generally written in tensor form like

$$\mathbf{T} + \zeta \frac{\partial}{\partial t}\mathbf{T} = \eta(\nabla \mathbf{v} + (\nabla \mathbf{v})^T) := 2\eta \mathbf{D}$$

as ζ is defined as a proper constant (actually the reciprocal of relaxation time) and $\mathbf{D}$ is deformation rate tensor.

For nonlinear viscoelastic cases, UCM (Upper Convected Maxwell model), Oldroyd B, Giesekus, and Phan-Thien-Tanner (PTT) models are popular kinds in different ways of manipulating elastic stress contribution (see [7, 43]). In nonlinear viscoelastic models, the derivative of stress tensor $\mathbf{T}$ reads in terms of upper convective form:

$$\mathbf{T}^{\nabla} := \frac{\partial}{\partial t}\mathbf{T} + \mathbf{v} \cdot \nabla \mathbf{T} - (\nabla \mathbf{v})\mathbf{T} - \mathbf{T}(\nabla \mathbf{v})^T$$

with velocity field $\mathbf{v}$ imposed. This is the derivative with respect to time during the flow. In this manner, the UCM is written as

$$\mathbf{T}^{\nabla} + \zeta \mathbf{T} = 2\eta \mathbf{D}.$$

The PEC model (Partially Extensional Convected model), which will be highlighted in the rest of this work, belongs to the viscoelastic models. This model, first proposed by Larson [29], is a generalization of the Doi-Edwards model by including partial strand extension of molecules confined in a tube region in the interior of entangled polymer melts. Vasquez et al. incorporate this model to formulate a two Hookean-species network model (VCM model) for entangled micelles with long and elastic chains which can rupture into two chains ([54, 55]). Recently these kind of models turn out to be effective to probe shear banding (see [44, 45, 55]) when passing the relaxation time to infinity. This constitutive model includes a parameter of reciprocal of relaxation time as well as upper convected derivative. The whole relation will be given later.

1.5 Shear banding

Spatial inhomogeneity is simulated and analyzed for circular Couette flow in [55]. This inhomogeneity is produced by local shear banding events (i.e. an unyielded band is located beside a yield band) in concentrated wormlike micelles. Two models are considered: one involving PEC for two micelle species and another involving PEC for a longer chain species and UCM for a shorter chain species. The ratio of the relaxation time of the shorter chain species and longer chain species is taken small. Inhomogeneous flow profiles are obtained

by start up of steady shearing which forms shear banding for different local deformation. In this setting, there is a range of shear stresses corresponding to two regions with different shear rate behavior (essentially the "yielded" and "unyielded" states). At the interface, the deformation rates jumps from a small level to a large level. When stress diffusions are absent in both models, shear bands appear as a result of nonmonotone viscometric flow curve; the position of the interface depends on the flow history. As highlighted in the paper, if diffusions are added in the model, the features differ: plateau-like flow curves are observed and the location of the interface is independent of flow history (see Figure 2.4 from PEC model simulation [55]). For PEC+M model, the simulation displays a similar plateau.

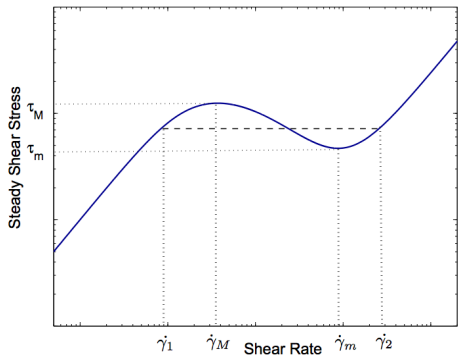

Figure 1.1: Shear banding: Non-monotonic viscometric prediction vs Plateau. The graph is directly from [55].

Several questions arise: Where is shear banding transition in reality? What mechanism governs it and how can we predict it? Although it is apparent that the nonmonotone dependence of shear stress on shear rate is the essential reason, the prediction of its precise location requires thorough discussion. With nonmonotone viscometric behavior and no regularizing mechanisms, the yield zone sharpens indefinitely as time goes on, and its eventual location corresponds to the maximum of the steady flow curve. Both of these conclusions are modified if we add higher order terms to the equations which may become important when the gradients of the conformation tensor become very large. Stress diffusion has widely been used as a regularizing mechanism in the literature [21, 31, 49, 55]. However, the stress diffusion employed in [55] has limitations because of its original assumption that particles carry their own stresses with themselves and that the precise mathematical consequences of stress diffusion are not easy to derive. An alternative mechanism based on an interfacial energy and Korteweg stresses has recently been proposed by Michael Renardy [45]. Such a theory was originally proposed by van der Waals [52] and Korteweg [28] for the liquid-gas transition and has also been used to model phase transitions in elastic solids (see e.g. [1, 2, 19, 20, 24, 25, 35, 51]). This theory begins with the assumption of interfacial energy which models density jump in the liquid-gas transition. In [45], a quadratic formulation of gradients of conformation tensor $\mathbf{C}$ defines the energy referred as tube misalignment energy.

When the transition happens or the interface forms, the interfacial energy effect is significant as gradients of $\mathbf{C}$ are not negligible; otherwise, it can be neglected as gradients of $\mathbf{C}$ are negligible. The Korteweg stress effect is from this energy; the stress depends on first and second gradients of the conformation tensor. The shear band location is found from an equal area rule similarly as the Maxwell's equal area rule predicted by van der Waals and Korteweg's work.

The formulation of interfacial energy is based on an assumption. Even if it is written as a quadratic form of tensor $\nabla\mathbf{C}$, it is still complicated to write up its full expression and analyze. So is the form of Korteweg stress. [45] gives the specific relation between interfacial energy and Korteweg stress with the specific assumption of parallel shearing when prescribing parallel steady shearing and will be briefly reviewed later.

1.6 A PEC model for thixotropic fluids

In this dissertation, we'll examine more closely a PEC model which is later used to study thixotropic fluids. We'll obtain yield stress behavior from a viscoelastic model by passing the limit of relaxation time to infinity. This approach was developed in recent work by Michael Renardy ([44]), in which the author invokes the Larson's PEC model to probe the salient properties of yield stress fluids with thixotropy.

Time scale separation is usual and essential in thixotropic flows. Basically, such behavior depends on a slow change of microstructure in apparent absence of deformation. The limit of large relaxation time grants such a separation of time scales. In the PEC model, the yield stress behavior arises naturally as a consequence of the model instead of being"built" into it. Singularly perturbed dynamical systems with "fast" and "slow" time scales arise in the analysis, indicating three fundamental asymptotic regimes, a fast elastic regime, a flowing yielded regime, and a slow dynamics, during which there is almost no obvious deformation while the microstructure gradually changes in slow evolution.

The analysis in [44] is for a simple shear flow driven by an imposed constant shear stress. Larson's PEC model now takes general differentiation form of a conformation tensor $\mathbf{C}$, which reads:

$$\mathbf{C}^{\nabla} + \epsilon(\phi(\operatorname{tr}\mathbf{C})\mathbf{C} - \chi(\operatorname{tr}\mathbf{C})\mathbf{I}) = 0. \tag{1.2}$$

The ratio ϵ of retardation time and relaxation time is assumed to be small as the relaxation time is supposed to be large. Consequently, the rate of change of the conformation tensor is small on the scale of ϵ unless the term multiplying ϵ is large. Furthermore, the stress tensor $\mathbf{T}$ is associated with $\mathbf{C}$ by multiplying a material function:

$$\mathbf{T} = \psi(\operatorname{tr}\mathbf{C})\mathbf{C}. \tag{1.3}$$

We assume that the total stress tensor $\mathbf{S}$ consists of the stress given by the PEC model as polymeric contribution plus a Newtonian stress with constant solvent viscosity η:

$$\mathbf{S} = \eta(\nabla\mathbf{v} + (\nabla\mathbf{v})^T) + \mathbf{T}. \tag{1.4}$$

Here, ϕ, ψ and χ are material functions of the variable $\mathrm{tr}(\mathbf{C})$ (the first invariant), which can be written arbitrarily. These different settings can lead to models which predict more thixotropic properties, such as PEC-Renardy model ([32]). We can see this kind of model as a modification of the upper convected Maxwell model (UCM) whose viscosity and relaxation time depend on the "structure parameter" $s = \mathrm{tr}\,\mathbf{C}$. With this interpretation, the model has a granted similarity with other efforts to model yield stress fluids; the main difference is that the modeling philosophy is a viscoelastic theory rather than a yield stress theory. The model in the form given above is similar to the dumbbell based models of dilute polymer solutions. The material functions are different from those typically used in that situation. For the PEC model, we specifically have $\phi(s) = \chi(s) = s + \alpha$, $\psi(s) = k/(s + \alpha)$ in which k is a stress modulus and $\alpha > -3$ is a dimensionless constant.

The parameter α is dimensionless. The quantity α is related to the size of the yield stress: the ratio of the elastic yield stress to the equilibrium stress modulus is $\sqrt{3+\alpha}/2$. Therefore, a large α corresponds to a high yield stress, while the limit $\alpha \to -3$ corresponds to a low yield stress. Larson's original theory requires α to be nonnegative. This is indeed consistent with data on the fluids for which the tube theory was intended, such as entangled polymers and wormlike micelles. On the other hand, such fluids as ketchup or clay pastes have rather short range interactions between particles and yield at pretty low strains. For such fluids, data fits [32] suggest a negative value of α. Rather remarkably, it turns out that in shear flows the parameter α does not affect the qualitative behavior of the system. We note that the value of α does affect elongational flow behavior [48]. Elongational data for wormlike micelles are consistent with a positive value of α [15]. On the other hand, elongational measurements for fluids which yield at low strain are difficult, and data are hard to find. In [33], it is noted that many yield stress fluids seem to obey a von Mises plasticity criterion (i.e. material does not flow until the second invariant of $\mathbf{D}$ exceeds a critical value. Furthermore, the elongation yield stress equals to $\sqrt{3}\tau_0$), which links the elongational yield stress to that stress in shear. The PEC model is consistent with this only if α is assumed close to -3, i.e. if the yield stress is small relative to the stress modulus.

In this work, we shall consider parallel shear flow. In such a flow, we have $C_{22} = C_{33} = 1$, $C_{13} = C_{23} = 0$, $s = C_{11} + 2$, and the PEC model reduces to

$$\begin{aligned} \dot{C_{11}} &= 2\kappa C_{12} + \epsilon(s+\alpha)(1 - C_{11}), \\ \dot{C_{12}} &= \kappa - \epsilon(s+\alpha)C_{12}. \end{aligned} \tag{1.5}$$

Here κ is the shear rate, the flow is in the "1" direction, and the velocity varies across the

"2" direction. If τ is the total shear stress, we have the relation:

$$\kappa := \frac{1}{\eta}\big(\tau(t) - T_{12}(t)\big) = \frac{1}{\eta}\big(\tau(t) - \frac{kC_{12}(t)}{s(t)+\alpha}\big). \tag{1.6}$$

The parameter k has the dimension of stress and the linear stress modulus is equal to $k/(3+\alpha)$. We shall nondimensionalize stresses by scaling with k, so we shall set $k = 1$ in the following content. Moreover, we shall scale time with η/k, then we are able to set $\eta = 1$. The parameter ϵ is then a dimensionless quantity proportional to the reciprocal of relaxation time. We can also eliminate α from the equations. Specifically, if we scale C_{12} with $\sqrt{3+\alpha}$, $C_{11} - 1$ with $3+\alpha$, τ with $1/\sqrt{3+\alpha}$, time t with $3+\alpha$ and ϵ with $(3+\alpha)^{-2}$, then α scales out. For the rest of this manuscript, we set $\alpha = 1$.

We note that the PEC model and its refined version, the VCM model, have been used to analyze large amplitude oscillatory shear flows of wormlike micelles [16, 56]. However, these papers' results are obtained for imposed (nominal) strain rather than stress. In prescribed strain experiments, the shear rate becomes inhomogeneous as soon as yielding occurs, leading to the appearance of shear bands. The analysis of these experiments is more complex that the analysis of homogeneous shear flows. Since this dissertation will focus on prescribed stress experiments, there are no experiments for us to compare our results. Comparisons for the PEC model (which is solved by computations rather than using asymptotics) for wormlike micelles are given in [56]. Some qualitative similarities are shared with this dissertation. We'll find a range of stress amplitudes and frequencies in which solutions are not unique and both yielded and unyielded states are possible. In comparing with [56], it should be noted that frequencies of order 1 are of order ϵ in ours. [56] sets parameter $\xi = 0.7$ and $\beta = 0.005$ to fit experimental data; in our notation $\alpha = 3/\xi - 3$, leading to $\alpha = 1.286$. Moreover, their β is the ratio of yielded to unyielded viscosity; in our dimensionless formulation, with α set to 1, β is 16ϵ. So $\beta = 0.005$ corresponds to approximately $\epsilon = 0.0003$. I.e. data for wormlike micelles agree with taking the limit of small ϵ. Indeed, fluids displaying spurt and shear banding usually have a viscosity changes of more than two orders of magnitudes. The role of a small parameter associated with this has not been exploited in the literatures. In [17], prescribed stress experiments for yield stress fluids are considered; however the studied object is Carbopol, which shows little or no thixotropy and is not fit for the case of the model considered here.

The asymptotic analysis of solutions to (1.5) as the relaxation time passes to infinity involves the interplay of several dynamic regimes. The simplest version of these is obtained by neglecting ϵ terms. We would refer to the resulting limit to as "fast" dynamics. On the other hand, there are two potential reasons why the neglected ϵ terms become relevant:

1. The observation time is long (of order $1/\epsilon$). Then even though the short term effect of the ϵ term is negligible, its cumulative effect must be considered. This regime will be referred to as "slow" dynamics.

2. The components of $\mathbf{C}$ are large, so even if ϵ is small, it is multiplied by a large number in the system. This regime is referred to "yielded" dynamics.

In M. Renardy's [44], the starup of shear flow was considered. That is, we start from an initial condition $C_{12} = 0$, $C_{11} = 1$ as rest state. As the constant shear stress τ is prescribed, the evolution of flow follows the solution of (1.5). The fluid behavior based on different range of constant τ is summarized and useful in analysis of shear bands formed in steady shearing as follows:

1. If $\tau > T_{12}^e := 1/4$, fast yielding occurs. The dynamics transition from fast to yielded dynamics happens eventually.
2. If $\tau < T_{12}^M := 1/(4\sqrt{2})$, slow dynamics reaches equilibrium, and the flow remains unyielded.
3. If $T_{12}^M < \tau < T_{12}^e$, delayed yielding occurs. The dynamics switches from fast to slow dynamics, but after a long time of slow evolution (order $1/\epsilon$), there is another transition from slow to fast and then to yielded dynamics.

This dissertation will partly be on the analysis of shear banding formed by the start up of planar Poiseuille flow. In this parallel flow, the shear bands occur since the flow covers a range of stress values leading to different behaviors as discussed above. The flow is in the x direction, and the velocity varies in the y direction (in the index notation used above, these direction correspond to index 1 and 2, respectively). Assuming negligible inertia, the momentum balance is given by

$$\frac{\partial \tau}{\partial y} = \frac{\partial p}{\partial x}. \tag{1.7}$$

If Q is the imposed pressure gradient, we therefore have $\partial\tau/\partial y = Q$, and if the centerline of the channel is at $y = 0$, then $\tau = Qy$. Therefore, the Poiseuille flow with imposed pressure gradient is equivalent to a one-parameter family of problems with imposed shear stress; this imposed shear stress varies linearly with location in the 2 direction. We shall choose the imposed pressure gradient large enough to cause yielding near the channel walls, while at the center of the channel the shear stress is always zero and the material remains unyielded. A sharp transition layer forms which partitions yielded and unyielded regions. To interpret the behavior of this transition region, we need to analyze not just the temporal behavior of solutions for given τ, but also the variation of the solution with τ (see Figure 1.2). We can nondimensionlize length so that $Q = 1$, i.e. $\tau = y$. We therefore do not have to distinguish in the following chapters between the imposed shear stress and the location in the channel. We shall assume that the half width of the channel is at least $T_{12}^e = 1/4$, so that fast yielding will occur near the walls of the channel.

We note that flows will be analyzed in the similar context that stress is controlled while most experiments are strain controlled. On the other hand, in a stress controlled experiment which starts from the unyielded state, the fluid remains unyielded as long as this is possible, and will yield only if the imposed stress exceeds the maximum in the steady flow curve. In a strain controlled experiment, thixotropic yield stress fluids will exhibit shear banding with a homogeneous stress (see e.g. [36, 41]).

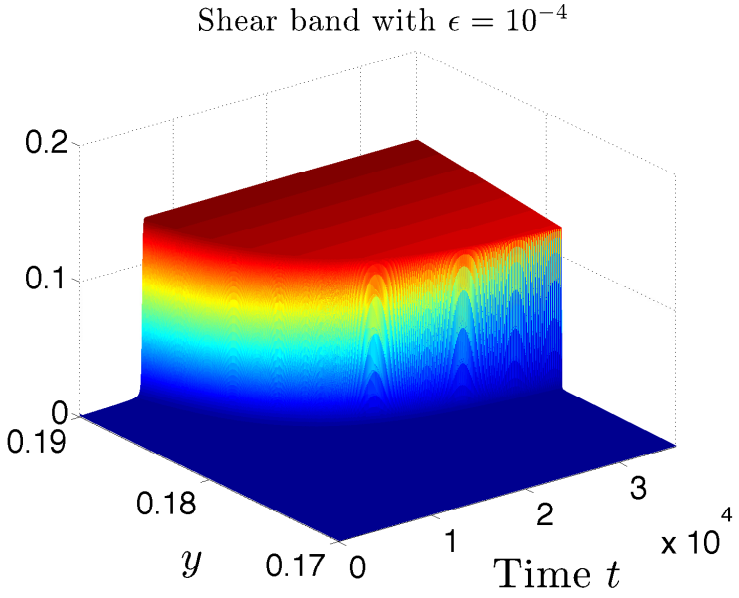

Figure 1.2: Shear banding simulated under prescribed shear stress for Poiseuille flow. At any time, the phenomenon is presented by a function of y or τ.

When Korteweg stress is included in the model in [45], the interfacial energy $W(\mathbf{C}, \nabla\mathbf{C})$ corresponding to (1.5) is specified as follows:

$$W = a_1(C_{11}, C_{12})(C'_{11})^2 + a_2(C_{11}, C_{12})C'_{11}C'_{12} + a_3(C_{11}, C_{12})(C'_{12})^2 \tag{1.8}$$

with coefficient $\mathbf{a} = (a_1, a_2, a_3)$. Here derivative notation $'$ refers to the derivative with respect to y. The Korteweg stress takes form as

$$\begin{aligned} T_K = {} & b_1(C_{11}, C_{12})C''_{11} + b_2(C_{11}, C_{12})C''_{12} + b_3(C_{11}, C_{12})(C'_{11})^2 \\ & + b_4(C_{11}, C_{12})C'_{11}C'_{12} + b_5(C_{11}, C_{12})(C'_{12})^2 \end{aligned} \tag{1.9}$$

with coefficients $\mathbf{b} = (b_1, b_2, b_3, b_4, b_5)$.

The relation connecting W and the Korteweg stress T_K is

$$W_t = T_K\kappa + j' + d \tag{1.10}$$

where j and negative definite d are functions of $C_{11},\ C_{12},\ C'_{11},\ C'_{12}$. According to a long calculation in [45], (1.9) has been derived from (1.8) with the specific relation between **a** and **b**. A proper assumption that $a_2 = 0$, $a_1,\ a_3$ are constant with $a_1 >> a_3$ is proposed as well following which our discussion will be around later.

1.7 Outline of this dissertation

In the next chapters (Chapter 2, 3, 4), the total shear stress $\tau(t)$ is set up to be periodic: $\tau(t) = A + B\sin(\omega t - \Phi)$. This setting-up involves four parameters A, B, ω and Φ. One might imagine the cases where the amplitudes A and B are large and the frequency ω may be either large or small relative to ϵ. This would lead to a large range of possibilities for parameter options. We shall focus on three specific situations: oscillation with modulation, oscillation without modulation, and oscillation with slow frequency.

In Chapter 2 we consider the situation when the oscillation modifies an imposed average stress, i.e. A is nonzero and dominates over B. We find that the oscillation produces yielding. Moreover, the "slow" dynamics is different from that corresponding to a constant imposed stress in [44]: rather than a simple evolution on a slow time scale we look at a slow modulation for stationary position of the periodic oscillation. The averaging method plays an important rule in describing the equilibrium. Besides, we shall identify three basic regimes of the fast, slow and yielded dynamics.

In Chapter 3, we focus on the cases under purely oscillatory forcing, i.e. $A = 0$. We will consider the cases where the frequency is of order 1.

Chapter 4 still deals with the pure oscillatory case with B of order 1, but large enough that a stress of this amplitude would induce yielding in a steady flow, and the frequency ω behaves like a power of ϵ: $\omega \sim \epsilon^p$. We shall see that the behavior for $p < 1/3$ is similar to $p = 0$; the system is described by fast dynamics within each oscillation, modulated by a slow dynamics. If $1/3 < p < 3/4$, the period of the oscillation is long enough to induce complete yielding, but not long enough for unyielding; the flow is completely described by yielded dynamics. If $p > 3/4$, the oscillation is slow enough to lead to a cycle of yielding and unyielding where the yielded state takes up most of the time. Section 4.5 discusses the assessment to what extent the material response is viscous or elastic. We shall pick the representative cases of frequency: $\omega = 1,\ \epsilon^{1/2}$ and ϵ corresponding to the three cases identified in previous sections in Chapter 4. The energy dissipation is calculated in a similar manner as in [17] for comparison.

Then we'll interpret the shear band phenomena by multiple scales.

Specially Chapter 5 focuses on planar Poiseuille flow driven by pressure. In this flow, inhomogeneity occurs among different locations on the 2 direction, i.e. the local stress is $\tau = y$ producing shear bands occurring at the region τ close to some values of τ. Multiscale analysis

is invoked to predict how the location of shear bands evolves with time. Moreover, computational simulations are used to validate the analysis. Seciton 5.4 is on planar Poiseuille flow setting considering the Korteweg stress effect. In this part, we may use the computation examples to illustrate an admissibility rule to predict the eventual exact shear band location. The Korteweg stress modifies the total stress to retard and smooth the cumulative sharpening effect from long time deformation and is significant when deformation state changes a lot along the 2 direction. In this context, the total stress is a superposition with not only Newtonian and polymeric contribution but Korteweg stress as well. The equal area rule is the admissibility criterion to predict the stationary shear banding location consistent with our simulation.

Chapter 2

Modulation of a stationary forcing

2.1 Fast dynamics

Setting $\epsilon = 0$ in the system, we obtain the shorter version of equations

$$\begin{aligned} \dot{C_{11}} &= 2\kappa C_{12}, \\ \dot{C_{12}} &= \kappa \end{aligned} \tag{2.1}$$

which is identified as fast dynamics. Multiplying the second equation by $2C_{12}$ and subtracting from the first, we obtain that

$$\frac{d}{dt}(C_{11} - C_{12}^2) = 0. \tag{2.2}$$

If we start from rest, where $C_{11} = 1$, $C_{12} = 0$, we therefore have

$$C_{11} - C_{12}^2 = 1, \tag{2.3}$$

which is the fast manifold. Along this curve, the fluid yields fast.

Due to the relation $s = \operatorname{tr} \mathbf{C} = C_{11} + 2 = 1 + C_{12}^2 + 2$, and noting that we have set $\alpha = 1$, from (2.1) we have

$$\dot{C_{12}} = \kappa = \tau(t) - \frac{C_{12}}{C_{12}^2 + 3 + \alpha} = \tau(t) - \frac{C_{12}}{C_{12}^2 + 4}. \tag{2.4}$$

We'll look at responses of fluids under different parameter settings in oscillations, i.e. we vary amplitude A, frequency ω, and phase Φ. All these responses will be shown via observing C_{12}.

2.1.1 A's influence when B is not big

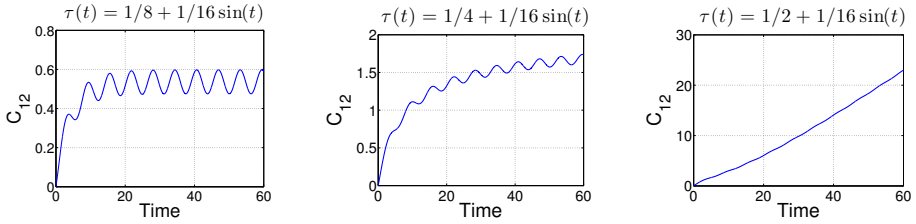

Figure 2.1: Plot of $C_{12}(t)$ for fast dynamics. The three graphs are responses of C_{12}, respectively, for $\tau(t) = 1/8 + 1/16\sin(t)$, $\tau(t) = 1/4 + 1/16\sin(t)$ and $\tau(t) = 1/2 + 1/16\sin(t)$. The first graph approaches a periodic solution, the other two continue to grow.

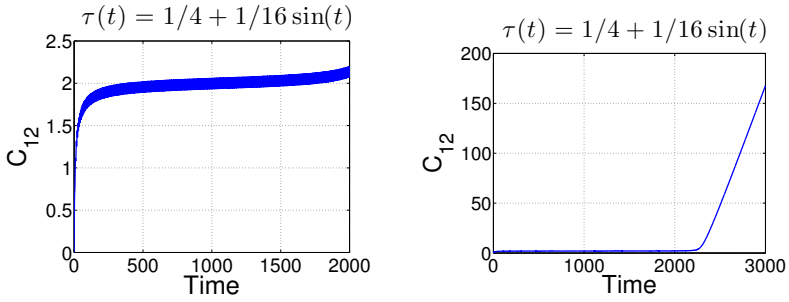

Figure 2.2: Plot of $C_{12}(t)$ for fast dynamics. $\tau(t) = 1/4 + 1/16\sin(t)$ propels C_{12} to be yielded.

If a constant shear stress $\tau = A$ is imposed, the fast dynamics will propel flow to yielding ([44]) provided that τ is larger than the maximum value of polymeric stress $C_{12}/(C_{12}^2 + 4)$, i.e.

$$\tau > T_{12}^e = \frac{1}{2\sqrt{3+\alpha}} = \frac{1}{4}. \tag{2.5}$$

Figure 2.1 shows solutions where τ is of the form $\tau(t) = A + B\sin(t)$, with $B = 1/16$ and various values of A. The solution for $A = 1/8$ approaches a periodic oscillation, while for $A = 1/2$, we have unbounded growth. The case $A = 1/4$ would be critical if $B = 0$ while the oscillation leads to yielding. This is shown more clearly in Figure 2.2. It appears at first as if C_{12} settles around the equilibrium value for nonoscillatory forcing, but eventually it grows.

A smart way to judge whether fast dynamics produces periodic solutions or not is to consider the solution of (2.4) with an arbitrary initial condition $C_{12}(0)$. For a periodic solution we would have $C_{12}(2\pi) = C_{12}(0)$. We therefore plot a graph of $C_{12}(2\pi)$ versus $C_{12}(0)$. If this curve crosses the diagonal of the first quadrant, the corresponding solution is periodic. If the curve is tangent to the diagonal, it is the critical case. The last case is that it misses the diagonal, which implies there is no periodic solution; this is the yielded case. These pictures

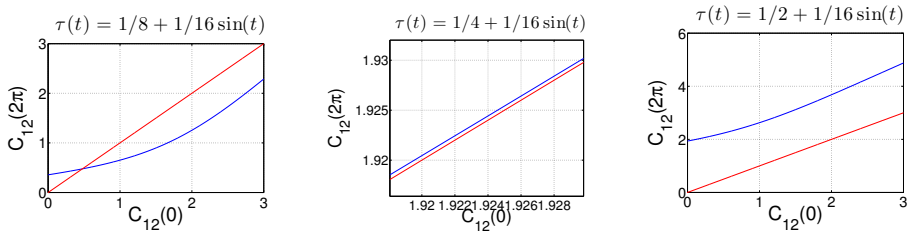

Figure 2.3: These three graphs show $C_{12}(2\pi)$ versus $C_{12}(0)$ for, respectively, the cases of $\tau(t) = 1/8 + 1/16\sin(t)$, $\tau(t) = 1/4 + 1/16\sin(t)$ and $\tau(t) = 1/2 + 1/16\sin(t)$ corresponding to unyielding (curve intersects the diagonal), near critical (tangent to diagonal) and yielded (curve misses the diagonal) state.

are shown in Figure 2.3. For $A = 1/4$, we have a "near miss," i.e. the fluid yields but just barely.

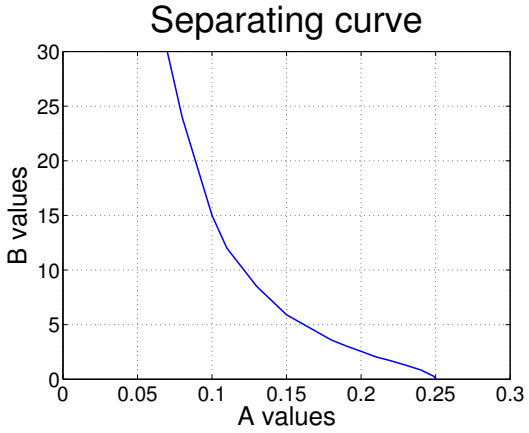

Figure 2.4: The upper part is yielding and the lower part is not yielding

It is of interest to point out the region where fast dynamics produces yielding. This is shown in Figure 2.4. Above the curve, yielding occurs. At $A = 1/4$, which is critical without oscillation, any oscillation however small will produce yielding. As A is decreased, the critical amplitude of the oscillation increases. In general, we see that the oscillation promotes yielding. This is consistent with the familiar observation that shaking a ketchup bottle promotes flow. Based on this observation, we can propose a heuristic argument based on the equation (2.4). For an unyielded flow, this equation has a periodic solution. For such a solution, the temporal average of $C_{12}/(C_{12}^2 + 4)$ must be equal to the average of τ, i.e. A. We note that the maximum value of the function $C_{12}/(C_{12}^2 + 4)$ is $1/4$, achieved at $C_{12} = 2$. Therefore the intuitive threshold for yielding under constant stress is at $A = 1/4$. If an oscillation is added, then the average of $C_{12}/(C_{12}^2 + 4)$ must be strictly less than the maximum value $1/4$ and the threshold for yielding decreases.

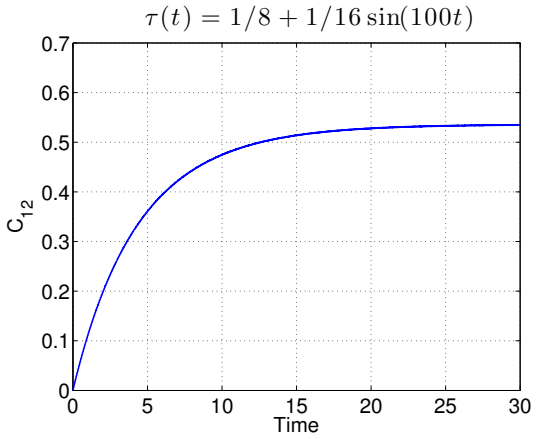

Figure 2.5: Simulations for $\tau(t) = 1/8 + 1/16\sin(100t)$. C_{12} is close to a fixed point, which can be derived from the averaged equation. Oscillations about this fixed point are small.

2.1.2 Fast frequency ω

Up to now, we have simulated the system and exhibited some dynamics under $\tau(t) = A + B\sin(t)$. It is of interest as well to investigate the influence of the frequency. If ω is of order one, the fast system displays similar oscillatory phenomena as when $\omega = 1$. If ω is very small, the fast system will behave like the system for constant shear stress, with a slow modulation. We will return to this small ω case for purely oscillatory forcing in Chapter 4. On the other hand, if ω is large, we have another separation of time scales, and we can analyze this by means of the averaging method. In this case, we rescale the time, i.e. we let $r = \omega t$, and we have the small parameter $\nu = \dfrac{1}{\omega}$. The fast system (2.1) becomes

$$\begin{aligned} \frac{d}{dr}C_{11}(r) &= 2\nu\kappa C_{12}(r), \\ \frac{d}{dr}C_{12}(r) &= \nu\kappa = \nu\Big(\tau(r) - \frac{C_{12}(r)}{C_{12}^2(r)+4}\Big). \end{aligned} \tag{2.6}$$

We cite an averaging theorem with a little modification from vector form to scalar form from Grimshaw's ODE text [26], Page 225, Theorem 9.3, which will be repeatedly used in the sequel.

Theorem 1. *Let a periodic non-autonomous system be given by*

$$\dot{u} = \epsilon F(u, t; \epsilon),$$

where F is periodic with respect to t with period 2π. The associated averaged system is defined by

$$\dot{U} = \epsilon \overline{F}(U, 0),$$

where

$$\overline{F} = \frac{1}{2\pi}\int_0^{2\pi} F(u,t;\epsilon)dt.$$

The averaged system approximates the original one on a time interval $0 \le \epsilon t \le C_0$, *in the sense that there is a constant* C_1 *such that*

$$|u(t) - U(t)| \le C_1\epsilon.$$

Here C_0, C_1 *are positive constants independent with* ϵ.

We apply this theorem to the system (2.6), with ν taking small magnitude analogous as the role of ϵ in the theorem, and C_{12} taking the role of u. The averaged equation is

$$\begin{aligned}\frac{d}{dr}\bar{C}_{12} &= \nu(-\frac{\bar{C}_{12}(r)}{\bar{C}_{12}^2(r)+4} + < \tau(r) >) \\ &= \nu(-\frac{\bar{C}_{12}(r)}{\bar{C}_{12}^2(r)+4} + A). \end{aligned} \tag{2.7}$$

The equilibrium point for our interest is given by a positive root of the right hand side.

For an illustrative example, let $\tau(t) = \frac{1}{8} + \frac{1}{16}\sin(100t)$, then

$$\frac{d}{dr}\bar{C}_{12} = \nu(-\frac{\bar{C}_{12}(r)}{\bar{C}_{12}^2(r)+4} + 1/8),$$

The equilibrium value is given by $\dfrac{\bar{C}_{12}}{\bar{C}_{12}^2+4} - 1/8 = 0$, leading to positive $\bar{C}_{12} = 0.535898$ fitting the simulation (see Figure 5.2) well. The equilibrium value of C_{11} is $\bar{C}_{11} = \bar{C}_{12}^2 + 1 = 1.2871867$.

At high frequency, our main observation is that the behavior is changed little from the case of no oscillation, i.e. the effect of the oscillation is negligible. Some pictures will be shown in Chapter 3 for pure oscillations.

To finish the discussion on parameter effects, we get to the last one: the phase Φ. We observe that different phases of the oscillation generally have little effect on the qualitative behavior. Some simulations will be shown for pure oscillations in Chapter 3. We omit corresponding simulation details here.

2.1.3 Thixotropy or not

We have so far shown results of fast dynamics on the evolution of the conformation tensor components. However, they are not directly measured in true experiment. What is measured

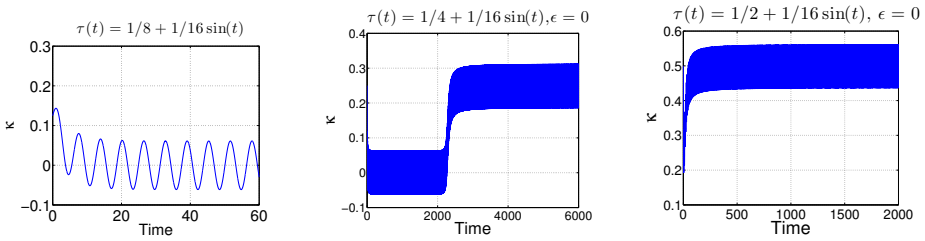

Figure 2.6: In unyielded flow κ oscillates around 0. In yielded cases, κ oscillates around a constant which is not 0.

in experiments is the shear rate κ and the Lissajous plots of flow curve for assessing the extent of thixotropy. Here we show some results for κ, to compare yielded and unyielded flows in this respect. The principal difference between yielded and unyielded states is that the average of κ is of order 1 in yielded states, but order ϵ in unyielded states. See Figure 2.6. In experimental work, it is common to show Lissajous plots. Such plots are in Figure 2.7. The second column shows the eventual periodic state. The shape is roughly elliptic for the unyielded case and close to a straight line in the yielded cases. The first column in the figure shows the complete transient starting from equilibrium. Note that for $t = 0$ we have $\tau = A$ and $C_{12} = 0$, hence $\kappa = \tau = A$. For the unyielded case ($\tau = 1/8 + \sin(t)/16$ in our simulation example), the shear rate decreases as polymeric stress $\dfrac{C_{12}}{C_{12}^2 + 4}$ builds up. In the yielded cases, there is an initial decrease of the shear rate, but ultimately this elastic stresses disappear as yielding occurs and the curve flow would be similar to that of a Newtonian fluid.

2.2 The slow dynamics

If fast dynamics leads to a periodic oscillation, then this periodic solution is, in general, a solution only to the fast dynamics. If we include the ϵ-terms, which have so far been neglected, then the periodic solution will gradually change over time with scale of order $1/\epsilon$. This gradual change is referred to slow dynamics. It will either lead to a truly periodic state (i.e. a solution of the full system) or to eventual yielding.

For the stationary case $B = 0$ in [44], it was shown that yielding on a slow time scale will occur if $A > T_{12}^M$. I.e. the time spent prior to eventual yielding increases and behaves as order of $1/\epsilon$ as A is decreased from $T_{12}^e = 1/4$ to $T_{12}^M = 1/(4\sqrt{2})$.

For the presence of oscillations, we can use the averaging method to analyze the slow dynamics. Let $u = C_{11} - C_{12}^2$. Our analysis of fast dynamics above is based on the fact that $\dot{u}$ is of order ϵ, thus we neglected it. To look closer to slow dynamics, we need to account the slow evolution of u. We obtain

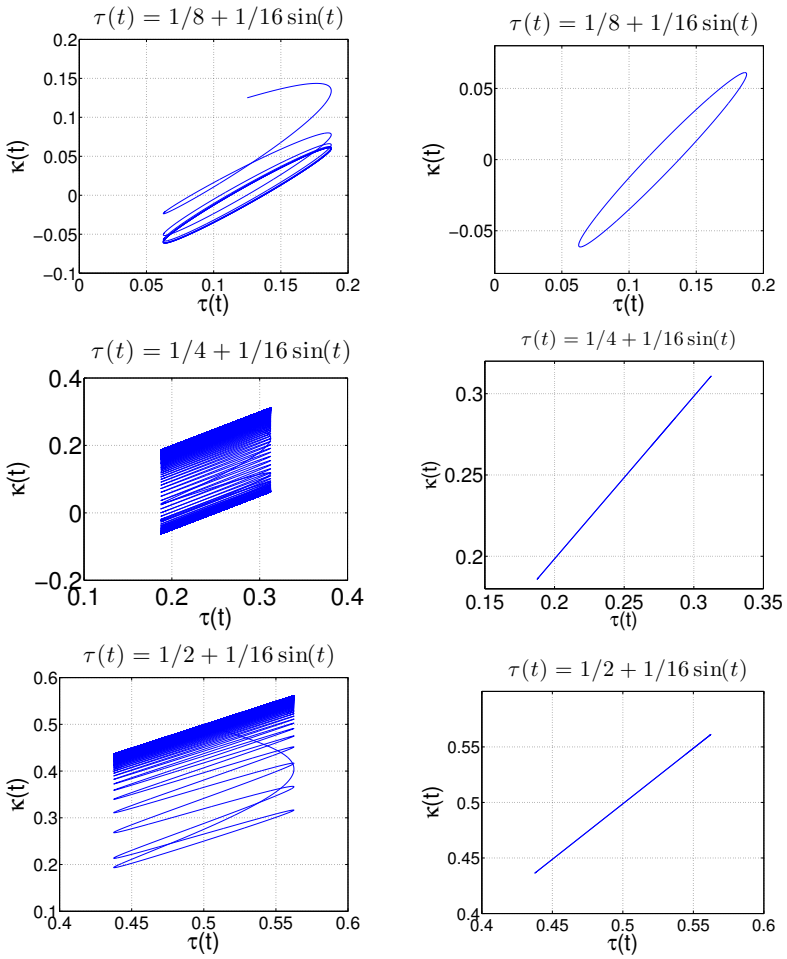

Figure 2.7: In unyielded flow, the picture is an ellipse while it is a line segment under the yielded flow. The ellipse is traversed in a clockwise direction. All plots in the first column start from the initial point (A, A).

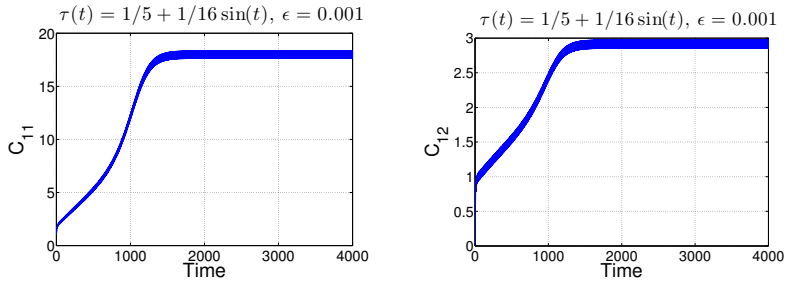

Figure 2.8: If $A = 0.2,\ B = 1/16$, a slow phase is followed by eventual yielding.

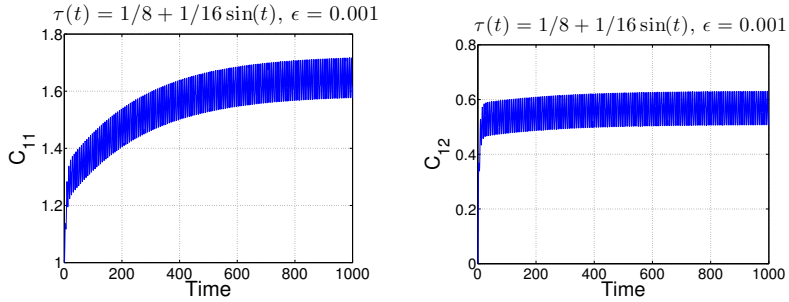

Figure 2.9: If $A = 1/8,\ B = 1/16$, the flow does not yield.

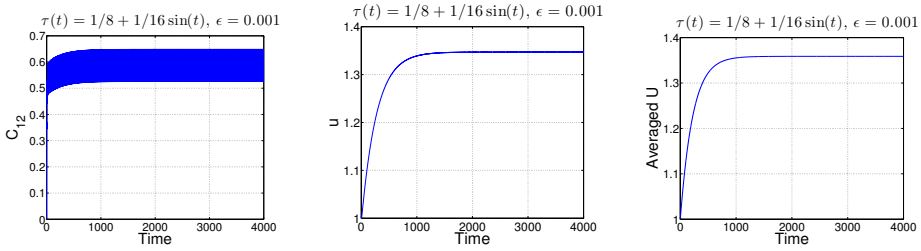

Figure 2.10: Here $\tau(t) = 1/8 + 1/16\sin(t)$, $\epsilon = 0.001$ and the time span for observing is of order $1/\epsilon = 1000$. The first two plots show $C_{12}(t)$ and $u(t)$, while the third plot shows the averaging approximation $U(t)$.

$$\begin{aligned} \dot{C}_{12} &= \tau(t) - \frac{C_{12}}{C_{12}^2 + u + 3} + O(\epsilon), \\ \dot{u} &= \dot{C}_{11} - 2C_{12}\dot{C}_{12} = \epsilon\phi(s)(1 - C_{11} + 2C_{12}^2) \\ &= \epsilon(C_{12}^2 + u + 3)(1 - u + C_{12}^2). \end{aligned} \tag{2.8}$$

Note that $\phi(s) = s+\alpha = C_{11}+3 = C_{12}^2+u+3$. In that $\dot{u}$ is of order ϵ, u will be approximately a constant over oscillations of $\tau(t)$. Slow dynamics is a regime, in which, for fixed u, the first equation of (2.8) has a stationary periodic solution. The actual solution will agree with this

stable periodic solution within order ϵ. We can then apply averaging to the second equation then we have

$$\dot{u} = \epsilon(C_{12}^2 + u + 3)(1 - u + C_{12}^2) = \epsilon(-u^2 - 2u + 3 + 4C_{12}^2 + C_{12}^4). \tag{2.9}$$

The averaging analysis consists in replacing C_{12}^2 and C_{12}^4 by their averages. Since we don't have closed form, we do not know this periodic solution C_{12} explicitly and have to compute it. We can obtain a reasonable approximation of the averages from a suitable truncation of C_{12}. At the crudest level of approximation, we approximate $C_{12}(t)$ as $a_0 + a_1\cos(t) + a_2\sin(t)$. Then algebra work gives

$$\begin{aligned} &< 4C_{12}^2 + C_{12}^4 >= 4 < C_{12}^2 > + < C_{12}^4 > \\ &= \big[\frac{8a_0b_1}{\pi} + 2a_0^2 + (a_1^2 + b_1^2)\big] + \frac{1}{2\pi}\big[8a_0^3b_1 + \frac{8}{3}a_0(3a_1^3b_1 + 2b_1^3) \\ &+ a_0^4\pi + 3a_0^2(a_1^2 + b_1^2)\pi + \frac{3}{8}(a_1^2 + b_1^2)^2\pi\big]. \end{aligned}$$

As an illustrative example, we set $\tau(t) = \frac{1}{8} + \frac{1}{16}\sin(t)$, and simulated the first equation of (2.8). Using cftool in Matlab, the output can be fitted by $C_{12}(t) = 0.5907 + 0.01794\cos(t) - 0.1217\sin(t)$. Therefore, we derive the averaged equation

$$\frac{d}{dt}U = \epsilon(-2U - U^2 + 4.56365), \tag{2.10}$$

which has a positive root at $U = 1.35874$. Figure 2.10 compares the evolution of the averaged variable $U(t)$ and a full simulation.

2.3 The yielded dynamics

To analyze the yielded case, we follow an idea from [44] and rescale C_{11}, C_{12} as $C_{11} = \epsilon^{-2/3}\tilde{C_{11}}$, $C_{12} = \epsilon^{-1/3}\tilde{C_{12}}$. Then

$$\begin{aligned} \frac{d}{dt}\tilde{C}_{11} &= 2\epsilon^{1/3}\tau(t)\tilde{C}_{12} - 2\epsilon^{2/3}\frac{\tilde{C}_{12}^2}{\tilde{C}_{11} + 3\epsilon^{2/3}} - \epsilon^{1/3}\tilde{C}_{11}^2 - 2\epsilon\tilde{C}_{11} + 3\epsilon^{5/3}, \\ \frac{d}{dt}\tilde{C}_{12} &= \epsilon^{1/3}\tau(t) - \epsilon^{2/3}\frac{\tilde{C}_{12}}{\tilde{C}_{11} + 3\epsilon^{2/3}} - \epsilon^{1/3}\tilde{C}_{11}\tilde{C}_{12} - 3\epsilon\tilde{C}_{12}. \end{aligned} \tag{2.11}$$

Neglecting terms of order smaller than $\epsilon^{1/3}$, we have (35) in [44]:

$$\frac{d}{dt}\tilde{C}_{11} = \epsilon^{1/3}(2\tau\tilde{C}_{12} - \tilde{C}_{11}^2),$$
$$\frac{d}{dt}\tilde{C}_{12} = \epsilon^{1/3}(\tau - \tilde{C}_{11}\tilde{C}_{12}). \tag{2.12}$$

It has a stable equilibrium $\tilde{C_{11}} = (2\tau^2)^{1/3}$, $\tilde{C_{12}} = (\tau/2)^{1/3}$ if τ is a constant. The small parameter $\epsilon^{1/3}$ motivates us to use the averaging method for the yielded system. The averaging method in this case simply leads to the same system where τ has been replaced by its average, i.e. a constant stress. Hence the effect of the oscillation becomes negligible. Comparisons of full simulations with the averaged results are given in Figures 2.11 and 2.12 to demonstrate the averaging analysis.

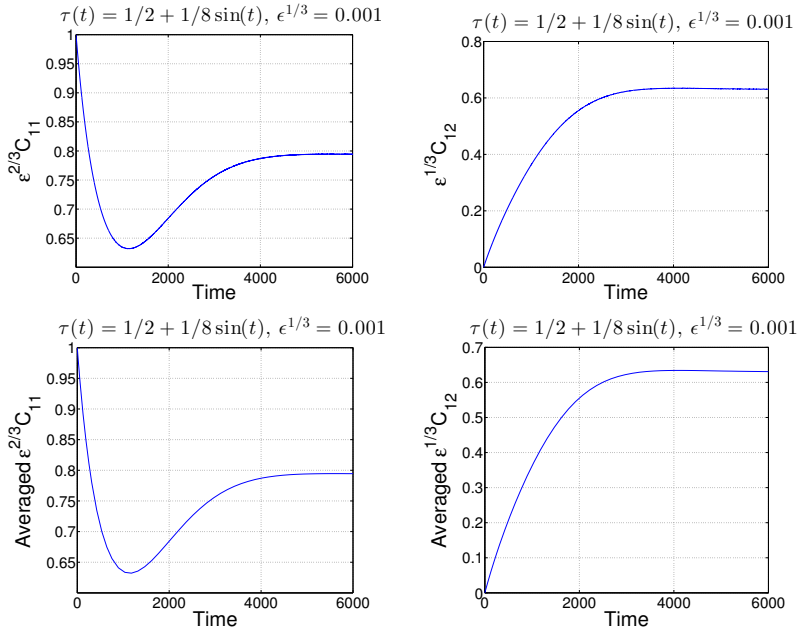

Figure 2.11: Here $\tau(t) = 1/2 + 1/8\sin(t)$, $\epsilon^{1/3} = 0.001$. The plot shows the rescaled variables $\epsilon^{2/3}C_{11}$ and $\epsilon^{1/3}C_{12}$. The second row shows the evolution of the averaged variables.

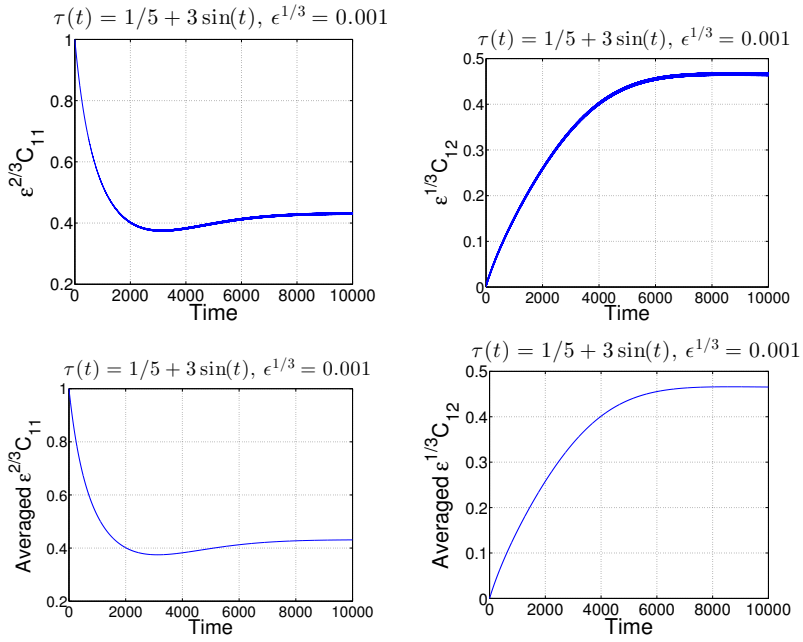

Figure 2.12: Here $\tau(t) = 0.2 + 3\sin(t)$, $\epsilon^{1/3} = 0.001$, the flow yields. The plot shows the rescaled variables $\epsilon^{2/3}C_{11}$ and $\epsilon^{1/3}C_{12}$. The second row shows the evolution of the averaged variables.

Chapter 3

Purely oscillatory forcing

In the simulation of the fast system above, the splitting curve in Figure 2.4 shows that if A is small, then the flow will yield only if B becomes pretty large. It leads to further discussion in this chapter. We shall focus on what happens if $A = 0$, i.e. the stress oscillation forcing the system has zero average. We will fix the frequency throughout this section, i.e. $\tau(t) = B \sin t$. We will observe the following behavior which is described by the following dynamics: When the amplitude B is small or of order 1, C_{12} immediately evolves into the stationary oscillation around the equilibrium 0. When B is large, C_{12} gradually evolves to oscillation around 0. The larger B is, the longer the time takes to reach the stable oscillation. When $B = O(\epsilon^{-1/2})$, the small terms neglected in the analysis for B of order 1 play roles, and a rescaling leads to a new asymptotic regime analogous to yielded dynamics above.

3.1 The fast system

Generally, when C_{12} is small, the solution to the C_{12} equation of the fast system (2.1) rapidly approaches stable oscillation around 0. The equation is linearized as

$$\frac{d}{dt}C_{12} = -\frac{1}{4}C_{12} + B\sin(t) \tag{3.1}$$

with the closed form solution

$$C_{12}(t) = C\exp(-\frac{t}{4}) + B\Big(\frac{4}{17}\sin(t) - \frac{16}{17}\cos(t)\Big). \tag{3.2}$$

On the other hand, if B is large, then C_{12} reaches large values in which the elastic stress $\dfrac{C_{12}}{C_{12}^2+4}$ can be neglected. Thus $\dfrac{d}{dt}C_{12}(t) \approx B\sin(t)$ and $C_{12}(t) \approx C - B\cos(t)$.

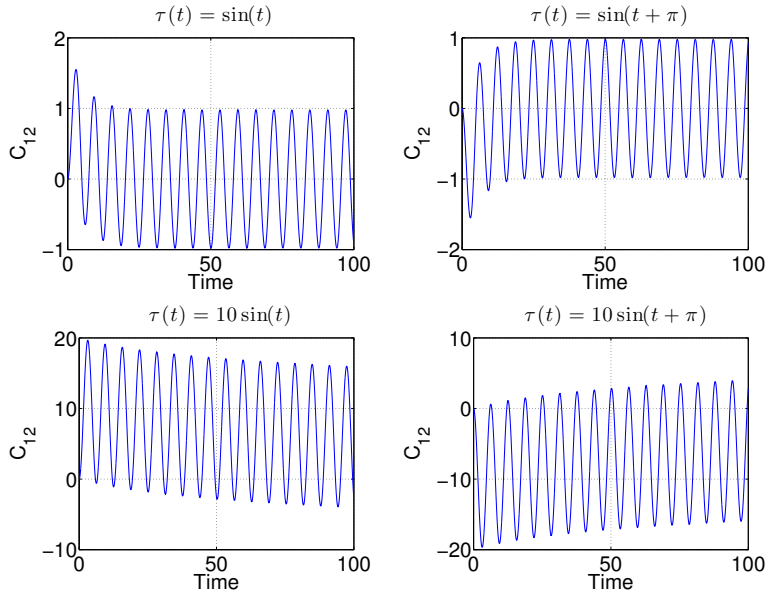

Figure 3.1: If $\tau(t) = \sin(t)$, then C_{12} quickly evolves to oscillation around 0. When B is larger, say 10, C_{12} still stably oscillates around 0, but after a longer time. If the phase of $\tau(t)$ is not zero, the flow eventually evolves to oscillation about 0 but the initial mean of oscillation is different.

Our simulations show a solution that initially oscillates about a nonzero mean depending on the phase of the imposed stress. During the evolution, the mean of the oscillation evolves to zero. The larger the amplitude, the longer it takes. This behavior is illustrated in Figure 3.1. We can see that in the fast dynamics, C_{12} represents the shear strain or deformation. If the flow were purely viscous, then there is no reason for the strain to reach zero mean, there would be a permanent offset depending on the direction in which you shear first. The larger the amplitude, the more "viscous" the behavior of the system becomes as elasticity becomes less important during longer time. Hence the time required to reach zero average increases.

3.2 Two "slow" systems

In the dissertation so far, the term "slow" referred to the full system with ϵ terms which lead to a gradual change on a large time scale. This analysis naturally extends to the case $A = 0$ and $B = O(1)$. As the manner analogous to Subsection 2.2, we obtain $C_{12}(t) = -0.9593\cos(t) + 0.2002\sin(t)$ as a fit when $\tau(t) = \sin(t)$ and $\epsilon = 0.001$. The averaged dynamics for $u(t)$ turns out to be

$$\frac{d}{dt}U = \epsilon(-2U - U^2 + 5.2665), \tag{3.3}$$

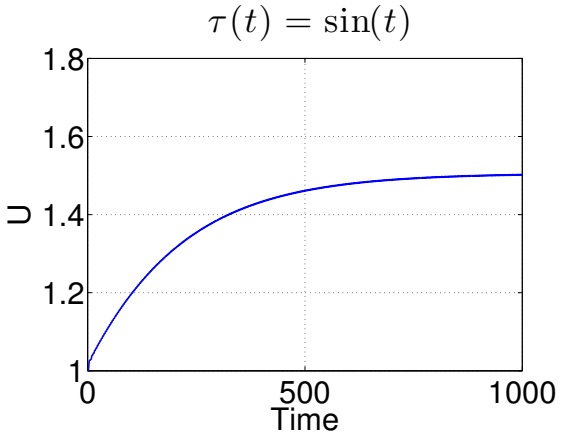

Figure 3.2: When $\tau(t) = \sin(t)$ and $\epsilon = 0.001$, $u(t)$ as given by (2.8) approaches 1.5033 when time goes to order $1/\epsilon$ in accordance with the equilibrium point of the averaged equation (3.3).

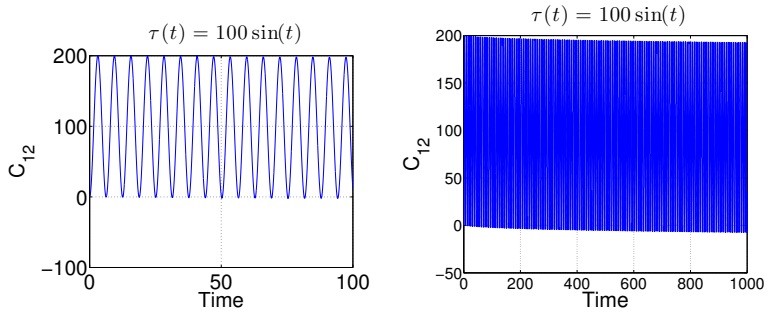

Figure 3.3: If $\tau(t) = 100\sin(t)$, the mean value of C_{12} decreases extremely slowly.

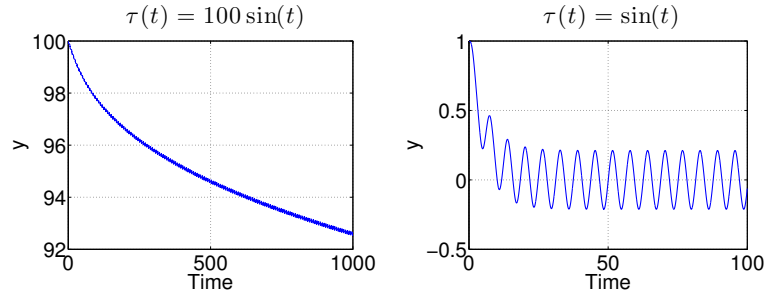

Figure 3.4: If $\tau(t) = 100\sin(t)$, i.e., $\nu = 0.01$, the mean value of $y(t)$ value gradually decreases and eventually oscillates around 0, which motivates us to simulate the averaged system of (3.4). If $\tau(t) = \sin(t)$, $y(t)$ decreases and quickly reaches stable oscillation.

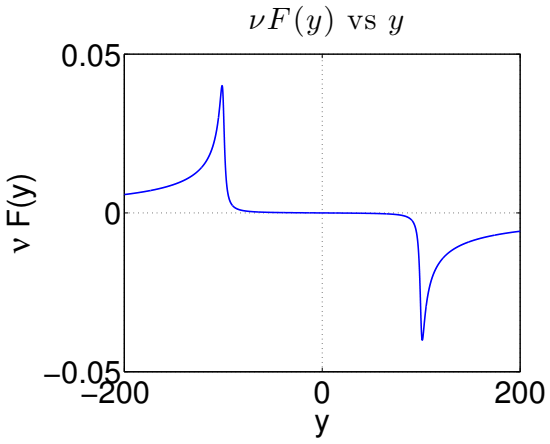

Figure 3.5: For $\nu = 0.01$, the right hand side of the averaged equation (3.5) is plotted versus y value. Clearly when $y = 0$, $F(0, \nu) = 0$.

leading to the fixed point 1.5033. The simulation for $u(t)$ of (2.8) as $\tau(t) = \sin(t)$ is given by Figure 3.2, which matches the average $U(t)$.

However, there is another slow regime which is a special case of the "fast" system in our terminology. Here, the flow takes a long time to obtain a stable mean when B is large. This regime shares with the previous one the fact that the stable equilibrium is still 0. See Figure 3.3. For this slow regime, the small parameter is denoted as $1/B$ other than ϵ, which is nearly zero. We assume $\tau(t) = B \sin t$, and we rewrite $C_{12}(t) = y(t) - B\cos(t)$ and then study $y(t)$. With this substitution, we have the initial value $y(0) = B$, and the equation (2.4) leads to the following equation:

$$\dot{y}(t) = -\nu \frac{\nu y(t) - \cos(t)}{[\nu y(t) - \cos(t)]^2 + 4\nu^2}, \tag{3.4}$$

where the parameter $\nu := \dfrac{1}{B}$. Figure 3.4 compares $B = 100$ and $B = 1$, showing that $y(t)$ takes a extremely long time to obtain stable oscillation predicted by Figure 3.3.

Specifically when B is very large, ν turns out to be very small as a perturbation parameter. We can therefore consider the averaged system:

$$\dot{y}(t) = -\frac{\nu}{2\pi} \int_0^{2\pi} \frac{\nu y(t) - \cos(s)}{[\nu y(t) - \cos(s)]^2 + 4\nu^2} ds := \nu F(y, \nu). \tag{3.5}$$

We note that we can't simply set $\nu = 0$ in this expression, since this blows up the integral. Nevertheless, averaging remains valid: Clearly the right hand side of (3.4) is small unless $\nu y - \cos t$ is small of order ν, which may lead the right hand side of (3.4) to be order 1.

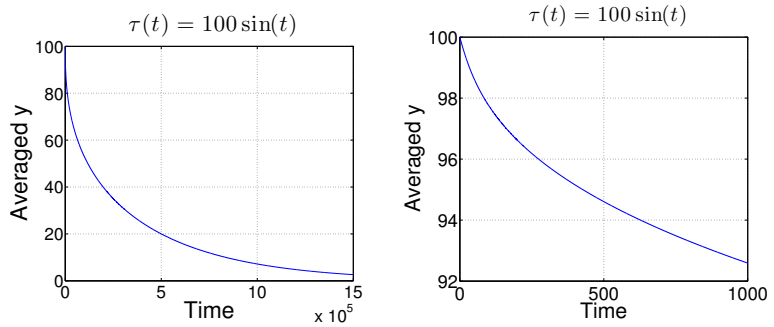

Figure 3.6: Solution of the averaged equation for the same parameters as used in Figure 3.4.

During one period of oscillation, $y\nu - \cos t$ can remain small as of order ν only over a time interval at most of order $\sqrt{\nu}$, and this is possible only if $y\nu$ is close to 1 or -1. In any case, the change in y during one period is therefore at most of order $\sqrt{\nu}$, and we are justified in regarding y as nearly constant.

We can obtain $F(y,\nu)$ using a closed form:

$$F(y,\nu) = -\frac{1}{4\pi}\int_0^{2\pi} \frac{1}{\nu y - \cos s + 2i\nu} + \frac{1}{\nu y - \cos s - 2i\nu}\, ds. \tag{3.6}$$

This complicated integral can be evaluated by the residue theorem and we just state the closed result. We set $z = \nu y$, and

$$p = \frac{1}{2}\Big(-1 - 4\nu^2 + z^2 + \sqrt{16\nu^2 z^2 + (1 + 4\nu^2 - z^2)^2}\Big). \tag{3.7}$$

Then we find the integral is

$$F(y,\nu) = -\frac{p^{3/2}}{p^2 + 4\nu^2 z^2}\mathrm{sgn}(y). \tag{3.8}$$

For fixed z and small ν , we find that p is of order one if $|z| > 1$, while of order ν^2 if $|z| < 1$. Hence $F(y,\nu)$ is of order 1 if $|z| > 1$ and of order ν if $|z| < 1$. Moreover, for $z = 1$, we find that p is of order ν and F of order $1/\sqrt{\nu}$. Moreover, $F(0,\nu) = 0$ gives that $y = 0$ is an equilibrium of the averaged equation. Figure 3.5 shows the behavior of F for a small value of ν and the peaks near $y = \pm 1/\nu$. Figure 3.6 shows the solution of the averaged equation for the same parameters as in Figure 3.4. The first one of the plot agrees with Figure 3.4; the second part shows the evolution over a longer time, illustrating eventual convergence to zero.

3.3 A rescaled system when $B = O(\epsilon^{-1/2})$

So far, we know that the system (2.1), namely fast dynamics, leads to a slow flow provided that B is large. However, for the original system (1.5), the small terms of order ϵ can no longer be neglected because of the existence of slow phase. Indeed, while this "slow dynamics" associated with fast dynamics having large B becomes slower as B is increased, the usual "slow dynamics" associated with small ϵ becomes faster, since ϵ is multiplied by terms which increase as B becomes larger. We could invoke the averaging method to both the elastic stresses and the ϵ terms to consider the two types of slow dynamics together. Eventually, for large enough B, the dynamics with the ϵ terms is no longer slow and actually possesses the same time scale as the fast dynamics. This is the regime we have already referred to as "yielded" dynamics.

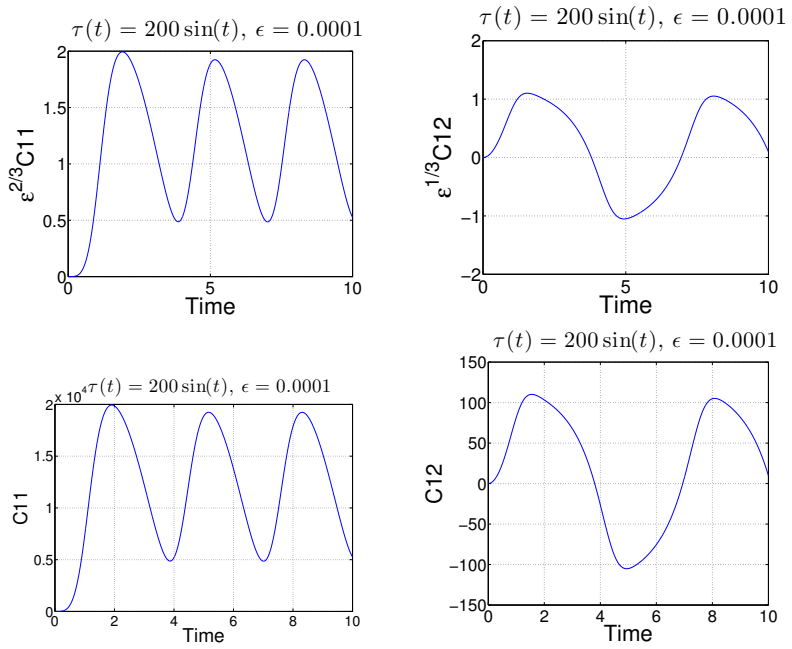

Figure 3.7: $\tilde{B} = 2$, i.e., $B = 200$ for $\epsilon = 0.0001$. $\tilde{C}_{11}$ quickly decreases from the initial value $\epsilon = 0.0001$ to around 1.25 approximately while $\tilde{C}_{12}$ oscillates around 0. Comparing to the simulation of full system, the only difference is the amplitude narrowing 10000 times and 100 times respectively for $\tilde{C}_{11}$ and $\tilde{C}_{12}$.

If B is large of order $\epsilon^{-1/2}$, it is possible to rescale our variables: Let $B = \epsilon^{-1/2}\tilde{B}$ and $C_{11} = \epsilon^{-1}\tilde{C}_{11},\ C_{12} = \epsilon^{-1/2}\tilde{C}_{12}$. The rescaled system is

$$\begin{aligned} \frac{d}{dt}\tilde{C}_{11} &= 2\tilde{B}\tilde{C}_{12}\sin(t) - \tilde{C}_{11}^2, \\ \frac{d}{dt}\tilde{C}_{12} &= \tilde{B}\sin(t) - \tilde{C}_{11}\tilde{C}_{12}. \end{aligned} \tag{3.9}$$

As a specific example, consider $\tilde{B} = 2$ and $\epsilon = 0.0001$, i.e. initially $\tau(t) = 200\sin(t)$. Figure 3.7 shows how the asymptotic equations behave with similar oscillation, comparing with the simulation of the full system. We emphasize that what we "rescale" is the amplitude, but time scale is not changed. Consequently the time needed to reach a stable state is of order 1.

Chapter 4

Pure oscillation with $\omega = \epsilon^p$

Up to now, the period of the oscillation has always been on the scale of the retardation time (i.e. 1 in dimensionless terms), which is much shorter than the time required for the fluid's yielding and unyielding. This is why we need a large amplitude to yield quickly, and we never saw a complete cycle of yielding and unyielding. In this chapter, we find out what happens for the sufficiently long period of the oscillation (slow frequency ω). We note that the material we study exhibits yield stress hysteresis, and unyielding happens over a much slower time scale than yielding [44]. The following will display this under relatively large amplitude oscillation.

We fix the amplitude of the total imposed stress at 1, i.e. $\tau(t) = \sin(\omega t)$, and $\omega = \epsilon^p$, where p is a positive number to get rid of potential effect from changing amplitude on yielding. We note that $1 > T_{12}^e = 1/4$, if p is large (very slow oscillation) such that the behavior is quasisteady, we can expect to observe a cycle of yielding and unyielding. Here quasisteady states mean the fluid behaves like steady state during a relative long time. Indeed, if $p > 1$, then the oscillation is sufficiently slow that a quasisteady state is reached at each time, and the dynamics simply traces the hysteresis curve for steady shear flow as in [44]. The following discussion will focus on the range $0 < p \leq 1$. We shall find that the fluid will be most yielded with a relatively short phase of unyielding when p is large.

4.1 The case $p < 1/3$

For $p < 1/3$, we have a behavior analogous to the case $p = 0$ discussed in the preceding section. We define $u = C_{11} - C_{12}^2$ as before, and we do the rescaling $r = \epsilon^p t$. With these substitutions, we obtain the system

$$\begin{aligned} \frac{dC_{12}}{dr} &= \epsilon^{-p}\Big[\sin(r) - \frac{C_{12}}{C_{12}^2+u+3} + O(\epsilon)\Big] \\ \frac{du}{dr} &= \epsilon^{1-p}(C_{12}^2+u+3)(1-u+C_{12}^2). \end{aligned} \tag{4.1}$$

This refers to "fast-slow" dynamics as in the previous section. During each cycle, we can treat u as an approximate constant, and C_{12} evolves according to the first equation. Now consider the first equation. Since the amplitude of the sine function is larger than the maximum of the function $f(C_{12}, u) := C_{12}/(C_{12}^2+u+3)$, C_{12} will oscillate with a large amplitude with order ϵ^{-p}. This is analogous to the large amplitude case in the previous section. To the leading order, we have $C_{12} = -\epsilon^{-p}\cos r$ for the stable oscillation with zero mean. In the second equation, we can average as in the previous chapter, i.e. the evolution of u is approximated by

$$\frac{d}{dr}U = \epsilon^{1-p}(-U^2 - 2U + 3 + 4\overline{C_{12}^2} + \overline{C_{12}^4}). \tag{4.2}$$

If we approximate $C_{12} \approx -\epsilon^{-p}\cos r$, we find that the equilibrium value of U is equal to $\epsilon^{-2p}\sqrt{3/8}$.

We confirm this behavior with a numerical example $p = 1/6$. Figure 4.1 shows the slow evolution from initial equilibrium when $\epsilon = 10^{-6}$. In Figure 4.2, we focus on the evolution of u. It approaches a mean of 61.42, demonstrating the prediction of $\epsilon^{-2p}\sqrt{3/8} = 61.24$. The Lissajous plot of κ versus $\tau(t)$ is close to a straight line, but still shows some deviation. An experimenter would characterize this state as "yielded"; indeed, viscous stresses dominate over elastic stresses. However, in terms of our dynamic classification we do not have "yielded" dynamics: the microstructure has not yielded to the point where it changes on the same time scale as the flow. See Figure 4.3 for the Lissajous plot and the elastic stress $C_{12}/(C_{11}+3)$.

In the analysis above, we saw that C_{12} is of order ϵ^{-p} and C_{11} is of order ϵ^{-2p}. If p exceeds $1/3$, we can no longer neglect the $O(\epsilon)$ term in the first equation of (4.1), since it gets multiplied by $C_{11}C_{12}$, which is now larger than $O(\epsilon^{-1})$. We thus expect to get into yielded dynamics. This case will be discussed in next section.

While the transition from fast-slow to yielded dynamics profoundly changes the manner of evolution of C_{11} and C_{12}, it does not have a major impact on the stresses, which are predominantly viscous not only for $p = 0$ but $p < 1/3$. So an experimenter measuring stress and shear rate would not see a dramatic change. This is a general issue in modeling thixotropic yield stress fluids: even when the microstructure contributes nearly nothing to the total stress, it has an impact on the future of the fluid, for instance the time the fluid takes to unyield if it is given a chance. An experiment probing this might be one where the oscillatory shear flow is stopped and subsequent unyielding is investigated.

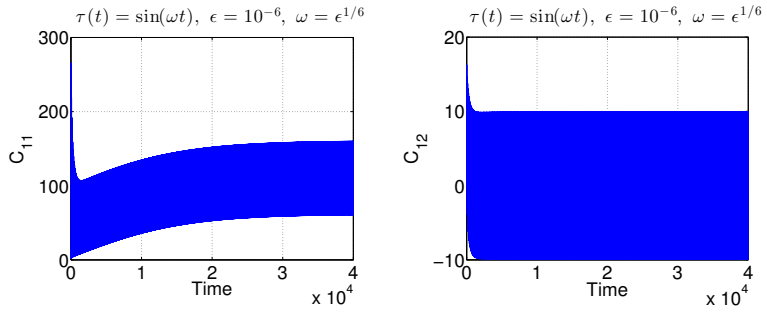

Figure 4.1: Evolution under slow oscillation $r = (\epsilon^{1/6}t)$, $\epsilon = 10^{-6}$.

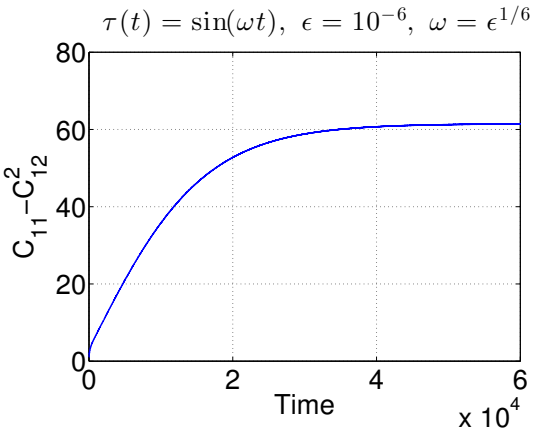

Figure 4.2: The value of u approaches 61.42, agreeing well with the prediction of averaging.

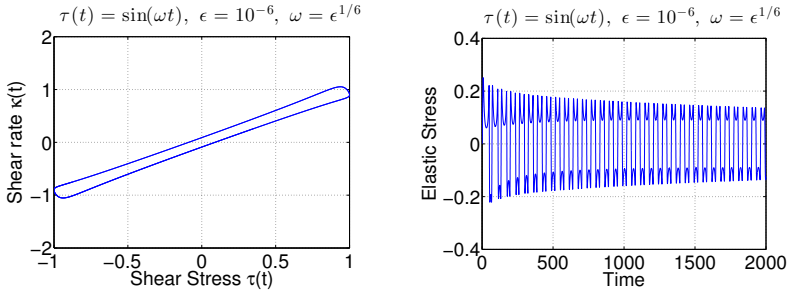

Figure 4.3: The Lissajous plot of κ versus $\tau(t)$ shows essentially yielded behavior for $r = (\epsilon^{1/6}t)$ and $\epsilon = 10^{-6}$, since the amplitude is large. Nevertheless, the dynamics of the microstructure is still "unyielded."

4.2 The case $1/3 < p < 3/4$

To describe yielded dynamics, we rescale $C_{11} = \epsilon^{-2/3}\tilde{C}_{11}$ and $C_{12} = \epsilon^{-1/3}\tilde{C}_{12}$. The rescaled system at leading order is as follows:

$$\begin{aligned}\frac{d}{dr}\tilde{C}_{11} &= \epsilon^{1/3-p}(2\sin(r)\tilde{C}_{12} - \tilde{C}_{11}^2),\\ \frac{d}{dr}\tilde{C}_{12} &= \epsilon^{1/3-p}(\sin(r) - \tilde{C}_{11}\tilde{C}_{12}).\end{aligned} \tag{4.3}$$

As $p > 1/3$, we expect a solution which can be approximated by setting the right hand sides equal to zero:

$$\begin{aligned}0 &= 2\sin(r)\tilde{C}_{12} - \tilde{C}_{11}^2,\\ 0 &= \sin(r) - \tilde{C}_{11}\tilde{C}_{12}.\end{aligned} \tag{4.4}$$

This leads to $\tilde{C}_{12} = (\sin r/2)^{1/3}$, $\tilde{C}_{11} = 2^{1/3}(\sin r)^{2/3}$.

The assumption that the derivative terms of (4.3) can be neglected is consistent until $\sin r$ is small on the same order as $\epsilon^{(3p-1)/5}$. At this moment, the derivatives play a role, i.e. the full system (4.3) must be considered. In fact, by taking derivatives of the solution of (4.4), we have, at the point where $\sin r \sim \epsilon^{(3p-1)/5}$

$$\begin{aligned}\frac{d}{dr}\tilde{C}_{11} &\sim \sin^{-1/3}(r) \sim \epsilon^{1/15-1/5p},\\ \frac{d}{dr}\tilde{C}_{12} &\sim \sin^{-2/3}(r) \sim \epsilon^{2/15-2/5p}.\end{aligned}$$

Meanwhile on the right side of (4.3), terms behave on the same scales, i.e. $\epsilon^{1/15-1/5p}$ or $\epsilon^{2/15-2/5p}$, respectively, for each equation.

(4.4) turns out to transition back eventually to quansisteady regime (4.4). We will show this transition in section 4.4.

On the other hand, we have to consider the possibility that the assumptions for the yielded dynamics don't hold while $\sin r$ is still large relative to $\epsilon^{(3p-1)/5}$. We note that the shear rate is given by

$$\kappa = \tau - \frac{C_{12}}{C_{11}+3}, \tag{4.5}$$

and in deriving yielded dynamics we neglect $C_{12}/(C_{11}+3)$. Hence yielded dynamics is no longer valid when this term cannot be neglected relative to $\tau = \sin r$. If C_{12} is of order

$(\sin r/\epsilon)^{1/3}$ and C_{11} is of order $(\sin r/\epsilon)^{2/3}$, then the two terms in the right hand side of (4.5) become of the same order when $\sin r$ is small of order $\epsilon^{1/4}$. We note that $1/4$ becomes less than $(3p-1)/5$, i.e. $\epsilon^{1/4} >> \epsilon^{(3p-1)/5}$ when $p > 3/4$. The dynamics will switch to a new regime different from the quasisteady regime (4.4) as $\sin(r) \sim \epsilon^{1/4}$. Therefore the fluid doesn't have a chance to get into the regime where derivatives are not negligible as $\sin(r) \sim \epsilon^{(3p-1)/5}$. In this sense, the yielded dynamics does not fully describe the behavior for $p > 3/4$. Actually unyielding occurs in this case, which will be considered in the next section. Furthermore we leave the part on analysis of how the dynamics goes back to quasisteady regime in section 4.4.

Figure 4.4 compares the yielded dynamics with the full dynamics of the full system when $\omega = \epsilon^{1/2}$.

Figure 4.5 shows essentially the yielded behavior with only small elastic stresses.

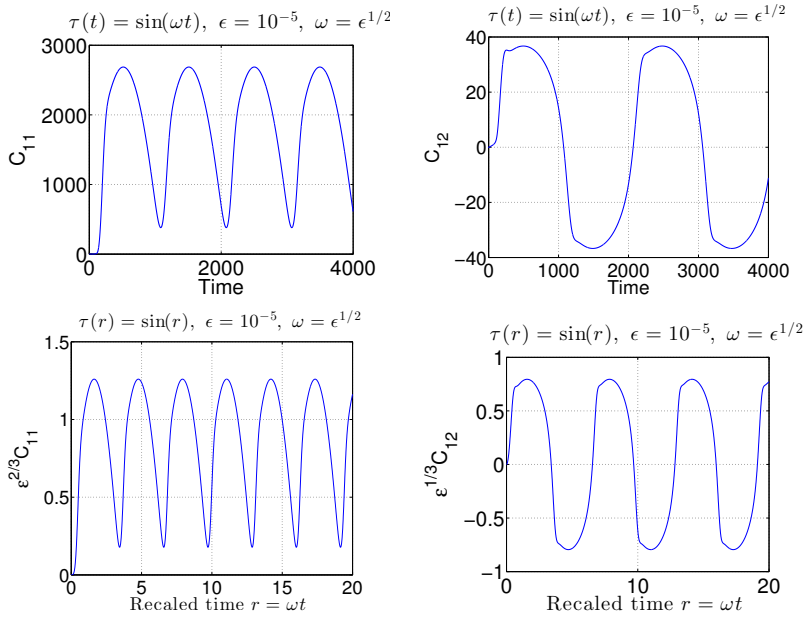

Figure 4.4: When $\omega = \epsilon^{1/2}$ with $\epsilon = 0.01,\ B = 1$, the system of yielded dynamics behaves similarly to the full system.

4.3 The case $p > 3/4$

Under this case, the stable oscillation is nevertheless described by the yielded dynamics as in the previous section but except vaguely when r becomes close to a zero of the sine function; for concreteness of the work, we shall in the following consider the case when r approaches the first positive root of the sine function , i.e. π without loss of generality. In the neighborhood of that zero: $r = \pi$, there is unyielding and subsequent yielding. The analysis of this process

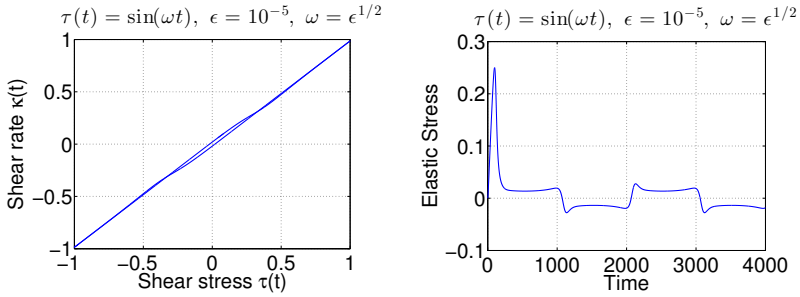

Figure 4.5: The behavior is essentially yielded.

is quite intricate and includes several stages, where we shall identify as Stages 1–4 below as different regimes in for the slow evolution of microstructure:

1. As pointed out at the end of the preceding section, yielded dynamics breaks down as $\pi - r$ becomes small of order $\epsilon^{1/4}$ while during the other time of a period, yielded dynamics prevails. At this point, elastic stresses become of the same order as viscous stresses and can't be neglected. The behavior remains quasistatic as it was in the yielded regime, i.e. the time derivatives of C_{11} and C_{12} can be of small order of ϵ power and hence neglected. The orders of magnitude of C_{11} and C_{12} are respectively $\epsilon^{-1/2}$ and $\epsilon^{-1/4}$ during this phase.

2. At a critical value $\bar{\sigma}$ of $(\pi - r)/\epsilon^{1/4}$, the existence of a quasisteady solution is lost. The flow then enters a new regime of more rapid phase during which $r = \pi - \bar{\sigma}\epsilon^{1/4} + O(\epsilon^{p-1/2})$. C_{11} and C_{12} decrease to order of magnitude $\epsilon^{p-5/4}$ and ϵ^{p-1}, respectively.

3. Then it is followed by a phase of slow evolution typical in [44], i.e. the shear rate is negligible, or $\tau = \sin r$ is balanced by the elastic stress $C_{12}/(C_{11} + 3)$ in the sense of leading order. Meanwhile, C_{11} is slowly decreasing. This phase persists until $r - \pi$ is of order ϵ^{1-p}. At this point, C_{11} has decreased to the order of magnitude ϵ^{2p-2}.

4. Finally, there is a yielding phase occuring over a short time scale. At the end of this phase, the system returns to the yielded dynamics.

4.3.1 Stage 1

The yielded dynamics already discussed above breaks down when $\pi - r$ or $\sin(r)$ becomes of order $\epsilon^{1/4}$. According to the yielded dynamics described above, C_{12} is at this time of order $(\pi - r)^{1/3}\epsilon^{-1/3} \sim \epsilon^{1/12}\epsilon^{-1/3} = \epsilon^{-1/4}$ and C_{11} is of order $\epsilon^{-1/2}$. This motivates a new rescaling

$$\begin{aligned} C_{11} &= \epsilon^{-1/2}\tilde{C}_{11}, \\ C_{12} &= \epsilon^{-1/4}\tilde{C}_{12}, \\ r &= \pi - \epsilon^{1/4}\sigma. \end{aligned} \tag{4.6}$$

At the leading order, the rescaled system is

$$\begin{aligned} \frac{d}{d\sigma}\tilde{C}_{11} &= \epsilon^{3/4-p}\big[2(-\sigma + \frac{\tilde{C}_{12}}{\tilde{C}_{11}})\tilde{C}_{12} + \tilde{C}_{11}^2\big], \\ \frac{d}{d\sigma}\tilde{C}_{12} &= \epsilon^{3/4-p}(-\sigma + \frac{\tilde{C}_{12}}{\tilde{C}_{11}} + \tilde{C}_{11}\tilde{C}_{12}), \end{aligned} \tag{4.7}$$

with derivative terms of order 1.

Since $p > 3/4$, it is natural to neglect left the hand sides and look for zeros of the resulting algebraic equation:

$$\begin{aligned} 0 &= 2(-\sigma + \frac{\tilde{C}_{12}}{\tilde{C}_{11}})\tilde{C}_{12} + \tilde{C}_{11}^2, \\ 0 &= -\sigma + \frac{\tilde{C}_{12}}{\tilde{C}_{11}} + \tilde{C}_{11}\tilde{C}_{12}, \end{aligned} \tag{4.8}$$

We can eliminate $\tilde{C}_{11}$ and obtain

$$\sigma = \frac{1}{2\tilde{C}_{12}} + 2\tilde{C}_{12}^3. \tag{4.9}$$

A solution of this equation exists only as long as $\sigma > \bar{\sigma} = 2\sqrt{2}/3^{3/4} \sim 1.24081$. When σ dips below $\bar{\sigma}$, the dynamics would switch to another regime toward the slow manifold.

4.3.2 Stage 2

When σ drops below $\bar{\sigma}$, the derivatives on the left hand side of (4.7) become large, and changes occur over a more rapid time scale. We can analyze this situation by replacing σ with the constant value $\bar{\sigma}$ on the right hand side of (4.7) and setting $\sigma = \bar{\sigma} + \epsilon^{p-3/4}\hat{\sigma}$ on the

left hand side. The outcome is an autonomous "time-backward" system

$$\frac{d}{d\hat{\sigma}}\tilde{C}_{11} = 2(-\bar{\sigma} + \frac{\tilde{C}_{12}}{\tilde{C}_{11}})\tilde{C}_{12} + \tilde{C}_{11}^2,$$
$$\frac{d}{d\hat{\sigma}}\tilde{C}_{12} = -\bar{\sigma} + \frac{\tilde{C}_{12}}{\tilde{C}_{11}} + \tilde{C}_{11}\tilde{C}_{12}, \tag{4.10}$$

The phase plane for this system is shown in Figure 4.6. To match to the preceding Stage 1, we need a solution that approaches the fixed point at $(\tilde{C}_{11}, \tilde{C}_{12}) = (3^{-1/2}, 3^{-1/4}2^{-1/2}) = (0.577, 0.537)$ as $\hat{\sigma} \to \infty$ (note that, according to substitution (4.6), σ and $\hat{\sigma}$ run "backward" in time). The phase plane plot shows precisely one such solution; this is the manifold connecting the fixed point to the origin. For $\hat{\sigma} \to -\infty$, this solution approaches the origin along the line $\tilde{C}_{12}/\tilde{C}_{11} = \bar{\sigma}$. We note that if we set $w = \tilde{C}_{12}/\tilde{C}_{11}$, then (4.10) leads to

$$\frac{dw}{d\hat{\sigma}} = (w - \bar{\sigma})(\frac{1}{\tilde{C}_{11}} - 2w^2). \tag{4.11}$$

If we assume $\tilde{C}_{11}$ to be small, we see that indeed w will approach $\bar{\sigma}$ as $\hat{\sigma} \to -\infty$. This implies the slow manifold $\sin(r) = \dfrac{C_{12}}{C_{11}+4}$ analogous in [44]. In fact, the equilibrium state $w = \tilde{C}_{12}/\tilde{C}_{11} = \bar{\sigma}$ leads to $C_{12} \sim (C_{11}+3)\sin(\omega t)$ if recovering all the scales.

4.3.3 Stage 3

Following this transition, the system enters a regime of slow dynamics before $(\tilde{C}_{11}, \tilde{C}_{12})$ arrives to the singular point $(0,0)$. During the slow regime, κ is small order of ϵ power, which implies $C_{12} \sim (C_{11}+3)\sin(\omega t)$ in accordance with small κ. By eliminating κ in the manner of [44], we find the equation

$$\frac{d}{dt}(C_{11} - C_{12}^2) = \epsilon(C_{11}+3)(1 - C_{11} + 2C_{12}^2). \tag{4.12}$$

If we use the approximation $C_{12} = (C_{11}+3)\sin(\omega t)$ as $\kappa \approx 0$, this becomes

$$\frac{d}{dt}(C_{11} - (C_{11}+3)^2\sin^2(\omega t)) = \epsilon(C_{11}+3)(1 - C_{11} + 2(C_{11}+3)^2\sin^2(\omega t)). \tag{4.13}$$

The consistency of the assumption of slow dynamics can be verified by looking at the evolution of $\kappa = \sin(\omega t) - C_{12}/(C_{11}+3)$. We find

$$\frac{d}{dt}\kappa = \omega\cos(\omega t) - \frac{(C_{11}+3-2C_{12}^2)\kappa}{(C_{11}+3)^2} - \epsilon\frac{4C_{12}}{C_{11}+3}. \tag{4.14}$$

The coefficient of κ on the right side is negative as long as

$$2C_{12}^2 < C_{11} + 3, \tag{4.15}$$

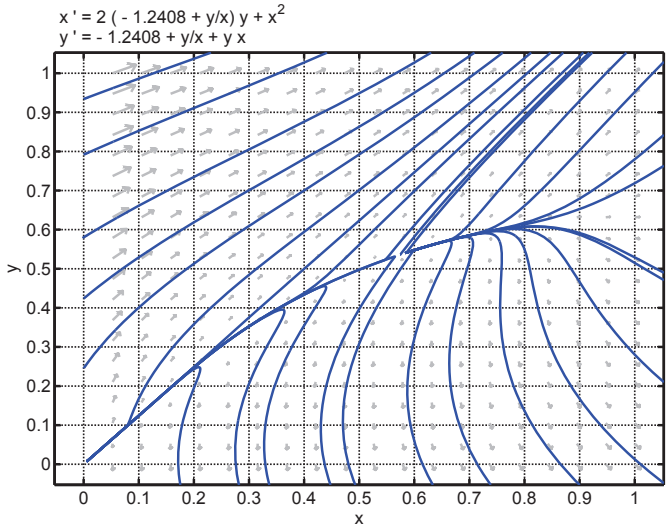

Figure 4.6: Phase plane for the autonomous system (4.10). The relevant solution curve emanates from the fixed point $(0.577, 0.537)$ and approaches the singular point at the origin. Moreover, the ratio $w = y/x$ approaches a constant when the trajectory approaches $(0, 0)$.

and other terms on the right hand side of (4.15) are small. Then κ will remain decreasing and small as long as (4.15) holds. If (4.15) fails, then slow dynamics breaks down.

In fact, slow dynamics starts at the point $\sin(\omega t)$ of order $\epsilon^{1/4}$ and the ratio C_{12}/C_{11} of order $\epsilon^{1/4}$. At this point, the leading order terms in (4.13) given the exact dynamics:

$$\frac{dC_{11}}{dt} = -\epsilon C_{11}^2, \tag{4.16}$$

which has close form of solution

$$C_{11} = \frac{1}{\epsilon t + K} := \frac{1}{\epsilon(t - (\epsilon^{-p}\pi - \epsilon^{1/4-p}\bar{\sigma}))}. \tag{4.17}$$

Matching to the previous phase (Stage 2) of the dynamics requires that $C_{11} \to \infty$ as $t = \epsilon^{-p}\pi - \epsilon^{1/4-p}\bar{\sigma}$, hence

$$K = -\epsilon^{1-p}\pi + \epsilon^{5/4-p}\bar{\sigma}. \tag{4.18}$$

If we set $\hat{r} = \epsilon^p t - \pi$, we find

$$C_{11} = \frac{1}{\epsilon^{1-p}\hat{r} + \epsilon^{5/4-p}\bar{\sigma}}. \tag{4.19}$$

According to the formulation of slow dynamics, $C_{12} \sim -\sin(\hat{r})(C_{11}+3)$. Hence C_{12}^2 reaches the same order of magnitude as C_{11} when $\hat{r}$ reaches the order ϵ^{1-p}. At this point, C_{11}, from (4.17), has decreased to order ϵ^{2p-2}.

As long as $p < 1$, we have only partial unyielding because C_{11} will still be at a large scale when slow dynamics breaks down (discussed in the next subsection). If $p = 1$, then C_{11} actually decreases to reach order 1. We must therefore modify the analysis as r becomes order ϵ^{-1} for we can no longer have $C_{11} >> 1$. We must then consider the full equation (4.13) instead of the truncated one.

4.3.4 Stage 4

Similar as in [44], slow dynamics breaks down when

$$\frac{d}{dC_{11}}(C_{11} - (C_{11}+3)^2\sin^2(\omega t)) = 1 - 2(C_{11}+3)\sin^2(\omega t) = 0, \tag{4.20}$$

since at this point slow dynamics would predict an infinite time derivative of C_{11}. This criterion coincides with (4.15). After this point is reached, the medium yields following a fast dynamics, where C_{12} and C_{11} grow and $C_{11} - C_{12}^2 = M\epsilon^{2p-2}$ is approximately constant. During this phase of fast dynamics, we can consider total stress τ approximately constant.

Since fast dynamics starts at the point where τ is of order ϵ^{1-p}, we shall set $\tau = K\epsilon^{1-p}$. Fast dynamics is then given by

$$\dot{C}_{12} = K\epsilon^{1-p} - \frac{C_{12}}{C_{12}^2 + 3 + M\epsilon^{2p-2}}. \tag{4.21}$$

We can scale ϵ out of this equation by setting $C_{12} = \epsilon^{p-1}\tilde{C}_{12}$, and $t = t_0 + \epsilon^{2p-2}\hat{r}$. Here t_0 is the time when slow dynamics breaks down, which is of order ϵ^{1-2p} according to the preceding discussion. The resulting equation is

$$\frac{d\tilde{C}_{12}}{d\hat{r}} = K - \frac{\tilde{C}_{12}}{\tilde{C}_{12}^2 + M(+3)}, \tag{4.22}$$

where the $+3$ term is present only if $p = 1$ and $C_{12}, C_{11} \sim 1$. For large $\hat{r}$, $\tilde{C}_{12}$ behaves like $K\hat{r}$. We have a return to the yielded dynamics, when $\epsilon C_{12}C_{11} \sim \epsilon C_{12}^3 \sim \epsilon^{3p-2}\hat{r}^3$ becomes of the same order as ϵ^{1-p}, i.e. when $\hat{r}$ is of the order $\epsilon^{1-4p/3}$. At this point, $t - t_0$ is of the order $\epsilon^{2p/3-1}$.

Figure 4.7 shows the dynamics for $\omega = \epsilon$. Yielded dynamics prevails during most of the period, but unyielding and subsequent yielding occur when the rescaled time passes through multiples of π whose sine value is 0. Figure 4.8 shows a magnification of this phase. Figure 4.9 shows that the flow has a pronounced unyielded state. The yielded state is still the main scenario during a period.

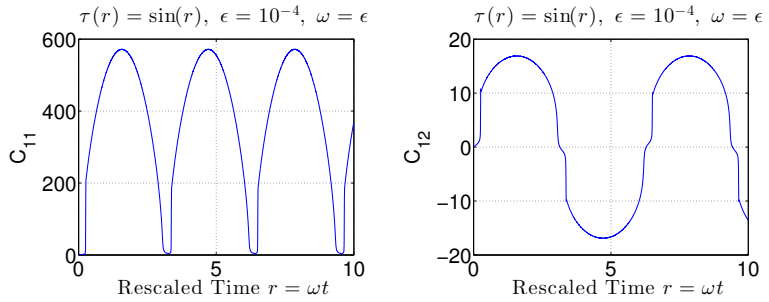

Figure 4.7: Evolution for $\epsilon = 0.0001$ with $\tau(t) = \sin(\omega t),\ \omega = \epsilon$. Time is rescaled with $1/\epsilon$. Yielded dynamics prevails over most of the period, but unyielding and subsequent yielding occur when the rescaled time passes through multiples of π.

4.4 "Back" transition when $1/3 < p < 3/4$

In this particular context, we discuss the dynamics when $\sin(r)$ evolves to $O(\epsilon^{\frac{3p-1}{5}})$. As we have discussed in section 4.2, the dynamics will evolve back to the quasisteady regime with negligible derivatives. This section aims to give a rigorous proof for this interesting transition.

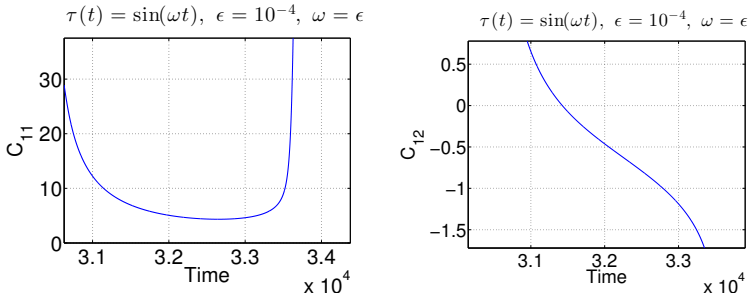

Figure 4.8: Magnification of the dynamics near $\omega t = \pi$ for Figure 4.7.

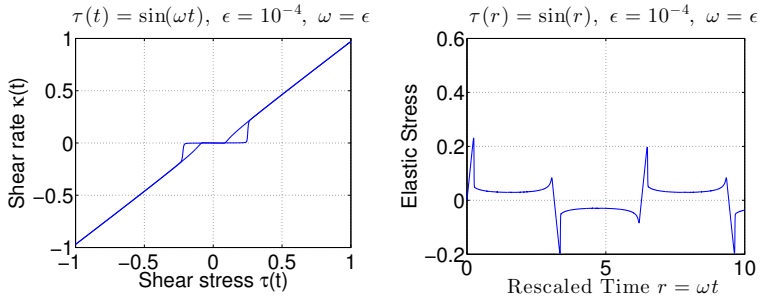

Figure 4.9: The flow goes through a cycle of yielding and unyielding.

Given the $\sin(r)$'s scale, $r - \pi \sim \epsilon^{\frac{3p-1}{5}}$ and the derivative terms play roles in the rescaled system. The scale behavior of constitutive components are $C_{12} \sim \epsilon^{\frac{p-2}{5}}$ and $C_{11} \sim \epsilon^{\frac{2p-4}{5}}$. Let rescale work as $C_{11} = \epsilon^{\frac{2p-4}{5}}\tilde{C}_{11}$, $C_{12} = \epsilon^{\frac{p-2}{5}}\tilde{C}_{12}$, and $\sin(r) = \epsilon^{\frac{3p-1}{5}}K$

thus

$$\epsilon^{\frac{2p-4}{5}}\frac{d}{dt}\tilde{C}_{11} = 2\epsilon^{\frac{3p-1}{5}}K \cdot \epsilon^{\frac{p-2}{5}}\tilde{C}_{12} - \epsilon \cdot \epsilon^{\frac{4p-8}{5}}\tilde{C}_{11}^2,$$
$$\epsilon^{\frac{p-2}{5}}\frac{d}{dt}\tilde{C}_{12} = \epsilon^{\frac{3p-1}{5}}K - \epsilon \cdot \epsilon^{\frac{2p-4}{5}}\tilde{C}_{11}\epsilon^{\frac{p-2}{5}}\tilde{C}_{12},$$

leading to

$$\frac{d}{dt}\tilde{C}_{11} = \epsilon^{\frac{2p+1}{5}}(2K\tilde{C}_{12} - \tilde{C}_{11}^2),$$
$$\frac{d}{dt}\tilde{C}_{12} = \epsilon^{\frac{2p+1}{5}}(K - \tilde{C}_{11}\tilde{C}_{12}).$$

Now rescaling the time $r - \pi = \epsilon^{\frac{3p-1}{5}}\tilde{r}$ and $\sin(r) = -\epsilon^{\frac{3p-1}{5}}\tilde{r}$, which implies $K = -\tilde{r}$, then $dt = \epsilon^{-p}dr = \epsilon^{-p+\frac{3p-1}{5}}d\tilde{r}$, therefore the rescaled system is

$$\frac{d}{d\tilde{r}}\tilde{C}_{11} = -2\tilde{r}\tilde{C}_{12} - \tilde{C}_{11}^2,$$
$$\frac{d}{d\tilde{r}}\tilde{C}_{12} = -\tilde{r} - \tilde{C}_{11}\tilde{C}_{12}. \tag{4.23}$$

The solution of this system will evolve to the quasisteady solution. I.e. $\tilde{C}_{11}$ and $\tilde{C}_{12}$ converge to $\sqrt[3]{2}\tilde{r}^{2/3}$ and $\frac{1}{\sqrt[3]{2}}(-\tilde{r})^{1/3}$ respectively as $\tilde{r} \to \infty$.

To justify this convergence, let $\tilde{C}_{11} = \tilde{r}^{2/3}x$ and $\tilde{C}_{12} = (-\tilde{r})^{1/3}y$, then from (4.23)

$$\frac{d}{d\tilde{r}}x = \tilde{r}^{2/3}(2y - x^2) - \frac{2}{3}\tilde{r}^{-1}x,$$
$$\frac{d}{d\tilde{r}}y = \tilde{r}^{2/3}(1 - xy) - \frac{1}{3}\tilde{r}^{-1}y.$$

As $\tilde{r} \to \infty$,

$$\frac{d}{d\tilde{r}}x = \tilde{r}^{2/3}(2y - x^2),$$
$$\frac{d}{d\tilde{r}}y = \tilde{r}^{2/3}(1 - xy). \tag{4.24}$$

Let $\hat{r} = \frac{3}{5}\tilde{r}^{5/3}$, an autonomous system is postulated in time variable $\hat{r}$. It is easy to check there is a stable fixed point $(\sqrt[3]{2},\ \frac{1}{\sqrt[3]{2}})$. Specially, the linearized system has the matrix at the fixed point:

$$\begin{pmatrix} -2\sqrt[3]{2} & 2 \\ -\frac{1}{\sqrt[3]{2}} & -\sqrt[3]{2} \end{pmatrix}$$

with positive determinant value and negative trace, which proves this fixed point is locally stable.

To see the orbit is globally attracted to this fixed point, we need to show the first quadrant of the phase plane is invariant. When the initial point is $(0, y)$ for any positive y, $\dot{y} = 1 > 0$ and $\dot{x} = 2y > 0$, hence the trajectory emitted from this point gets into the first quadrant. On the other hand, if the initial point is $(x, 0)$ for any x, $\dot{y} = 1 > 0$ and $\dot{x} = -x^2 \leq 0$ and the trajectory shoots in the first quadrant as well. Moreover, $x - y^2 \geq 0$ is invariant in that

$\frac{d}{dt}(x-y^2) = -x(x-y^2) + xy^2$ and if $x - y^2 = 0$, the right hand side of the equation is positive.

Second, to prove the global attraction is to prove the global boundedness of x and y. Since the trajectory starting from $(0, y)$ has always positive $\dot{x}$, there is a positive δ which x will evolve to exceed after a certain time. To assure that y is bounded, we could write out the implicit solution of $\dot{y} + xy = 1$. In fact, it can be written that

$$\frac{d}{dt}\big(\exp(\int_0^t x ds)y\big) = \exp\big(\int_0^t x ds\big),$$

taking integral over time $[0, t]$, then

$$y = \int_0^t \exp\big(\int_s^t -x d\alpha\big) ds + y_0 \exp\big(\int_0^t -x ds\big), \tag{4.25}$$

where y_0 is the initial value of y.

Given $x \geq \delta$,

$$\begin{aligned} y &\leq \int_0^t \exp\big(-\delta(t-s)\big) + y_0 \exp(-\delta t) \\ &= \int_0^t \exp(\delta s) ds \times \exp(-\delta t) + y_0 \exp(-\delta t) \\ &= \frac{1}{\delta}(1 - \exp(-\delta t)) + y_0 \exp(-\delta t). \end{aligned}$$

When t is large enough, $y_0 \exp(-\delta t) \leq \frac{1}{\delta}$, leading to $y \leq \frac{2}{\delta}$.

Similarly,

$$x = 2\int_0^t y \exp\big(-\int_s^t x d\alpha\big) ds + x_0 \exp\big(\int_0^t -x ds\big)$$

for center initial value x_0.

hence

$$\begin{aligned} x &\leq \frac{2}{\delta}\int_0^t \exp\big(-\delta(t-s)\big) ds + x_0 \exp\big(\int_0^t -x ds\big) \\ &= \frac{2}{\delta^2}(1 - \exp(\delta t)) + x_0 \exp(-\delta t), \end{aligned}$$

which leads to $x \leq \dfrac{3}{\delta^2}$ for sufficiently large t.

It is easy to check that there is no closed orbit in the first quadrant because the divergence of the system is negative.

As $\tilde{r} \to \infty$, i.e., $\tilde{r} \sim \epsilon^{-\gamma}$ for any small positive γ, $\tilde{C}_{11} = \sqrt[3]{2}\tilde{r}^{2/3}$ and $\tilde{C}_{12} = \dfrac{1}{\sqrt[3]{2}}(-\tilde{r})^{1/3}$ is the quasisteady solution while $\sin(r) = \epsilon^{\frac{3p-1}{5}}\tilde{r} \sim \epsilon^{\frac{3p-1}{5}-\gamma} >> \epsilon^{\frac{3p-1}{5}}$. Once $\gamma = -\dfrac{3p-1}{5}$, $\tilde{C}_{11} \sim \epsilon^{-\frac{2(3p-1)}{15}}$ and $\tilde{C}_{12} \sim \epsilon^{-\frac{3p-1}{15}}$, i.e., $C_{11} \sim \epsilon^{-2/3}$ and $C_{12} \sim \epsilon^{-1/3}$.

Therefore, the flow is quasisteady until $\sin(r) \sim \epsilon^{3p-1/5}$ when the equation loses its quasisteady solution. During short time $r - \pi \sim \epsilon^{\frac{3p-1}{5}}$, the solution is not quasisteady. Then the solution is attracted to its quasisteady solution and the flow gets back to the quasisteady state eventually.

4.5 Elastic versus viscous response and energy dissipation

It is instructive to assess what extent the response of the medium is elastic or viscous. The shear stress $\tau = B\sin(\omega t)$ is still imposed and a simulation is implemented for long enough so the system settles down to a harmonic response. We can then separate the periodic shear rate into an odd part representing a viscous response and an even part representing an elastic response from the harmonic response. This decomposition methodology is introduced for constitutive equations of linear and nonlinear viscoelasticity to explain the elastic and viscous moduli in [13]. The similar decomposition, however for the strain, is carried on in [17]. To simplify such expansions, we only look at the dominant Fourier mode of deformation rate (strain rate), i.e. the low frequency terms, which is to do a least square fit of $\kappa(t)$ as

$$\kappa(t) \sim \kappa_v \sin(\omega t) + \kappa_e \cos(\omega t). \tag{4.26}$$

Tables 4.1, 4.2, 4.3 show the results of such a decomposition as a function of amplitude. We have set in simulations $\epsilon = 10^{-4}$ and look at the cases $\omega = 1$, $\omega = \epsilon^{1/2}$ and $\omega = \epsilon$ to stand for three oscillatory cases in the previous sections. Not surprisingly, the behavior is viscous dominated for large amplitudes at all three frequencies. At small amplitude, the behavior tends to be elastic if $\omega = \epsilon^{1/2}$. At $\omega = \epsilon$ and $\omega = 1$, there is a viscous contribution even at small amplitudes though for different reasons: If $\omega = 1$, the Newtonian viscosity is effective, while $\omega = \epsilon$, stress relaxation takes roles. The tables for $\omega = \epsilon$ and $\omega = \epsilon^{1/2}$ show an obviously strong increase of κ_v between $B = 0.1$ and $B = 1$. This manifests the spurt that happens as yielding occurs. For $\omega = \epsilon$, we see a small negative value of κ_e at the larger

B	κ_{e}	κ_{v}	E_d
100	0.0145	99.99	3.146×10^4
50	0.0201	49.99	7.8524×10^3
10	0.0950	9.999	3.141×10^2
1	0.201	0.957	3.007×10^0
0.1	0.0235	0.0941	2.96×10^{-2}
0.01	0.00235	0.00941	2.96×10^{-4}

Table 4.1: $\omega = 1$

B	κ_{e}	κ_{v}	E_d
100	0.00488	99.99	3.141×10^6
50	0.00604	49.99	7.852×10^5
10	0.00944	9.981	3.136×10^4
1	0.0154	0.9587	3.011×10^2
0.1	0.00421	2.69×10^{-4}	8.40×10^{-3}
0.01	0.000398	3.185×10^{-5}	1.000×10^{-4}

Table 4.2: $\omega = \epsilon^{1/2}$

B	κ_{e}	κ_{v}	E_d
100	-0.00872	99.99	4.687×10^8
50	-0.00820	49.99	1.172×10^8
10	-0.0122	9.983	4.679×10^6
1	-0.0342	0.960	4.485×10^4
0.1	3.723×10^{-5}	1.834×10^{-4}	8.573×10^{-1}
0.01	3.972×10^{-6}	1.6×10^{-5}	7.5×10^{-3}

Table 4.3: $\omega = \epsilon$

amplitudes; we believe that these negative values result from yield stress hysteresis rather than elasticity.

As well, the tables show the energy dissipation from the viscous effect per period defined as

$$E_d = \int_{t_0}^{t_0+T} \tau(t)\kappa(t)\,dt.$$

We show the energy dissipation in a log-log plot in Figure 4.10. In a linear medium, the slope of the curve should be 2. We observe this at both high amplitudes (purely viscous behavior) and low amplitudes (linear viscoelastic behavior). At intermediate amplitudes, the slope becomes larger, reflecting the spurt as the fluid yields. At higher frequencies, the spurt disappears because the Newtonian viscosity is effective even in the unyielded state.

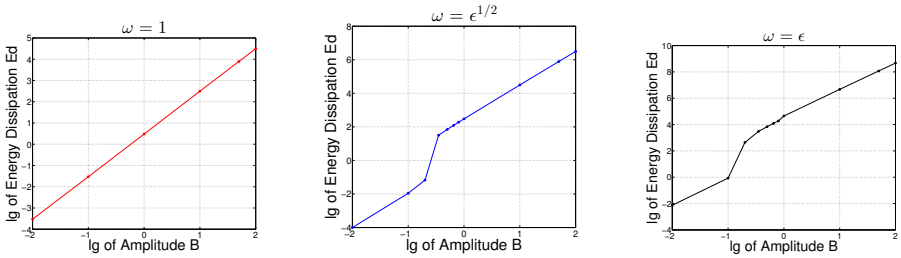

Figure 4.10: The energy dissipation of $\tau(t) = B\sin(t)$, $\tau(t) = B\sin(\epsilon^{1/2}t)$ and $\tau(t) = B\sin(\epsilon t)$ for different amplitudes B.

Chapter 5

Shear banding

The analysis in the chapter will focus on the steady shear flow. This flow, produced by planar Poiseuille flow (1.7), has spatial inhomogeneity and shear bands occur. That is the yielded and unyielded regions juxtaposed along the flow direction. It is of interest to figure out the band region (the transition or overlap region of two juxtaposing bands).

Our effort first focuses on the yield time, i.e. the time which passes between the initial start up of the flow and the time when the fluid yields. It is known that the yield time will be of order 1 if $\tau > 1/4$, of order $1/\epsilon$ if $1/(4\sqrt{2}) < \tau < 1/4$, and there is no yielding if $\tau < 1/(4\sqrt{2})$. A complicated analysis will be provided to figure out the specifics of the transitions between these regimes when τ is close to $1/4$ or, respectively, $1/(4\sqrt{2})$. We shall discuss different rescalings of the equations leading to some asymptotic regimes for these transition zones which manifest the behavior of shear bands in the PEC model.

In the final part of this chapter, we shall predict the realistic location of the shear banding transition. Corresponding to two different formulations of the free energy, there arise different Korteweg stresses in contribution of total stress. Computations are implemented for estimating that location using our theory.

5.1 How to analyze shear bands

Before analyzing these mechanisms in detail, let us formulate a problem by connecting the variation of the yield time as a function of y to the appropriately defined width of the transition between yielded and unyielded regions. We'll use these relations to connect the multiple scales to the shear banding.

Let $T(\tau, \kappa)$ be the time when the shear rate reaches value κ. We can choose κ to be a suitable value and identify the position of the yield zone at time T as the inverse function $\tau(T, \kappa)$. Let $K(\tau, t)$ be the shear rate at position τ and time t, then this shear rate is given by (1.6)

with C_{12}, C_{11} given by the solution of (1.5). Clearly, we have

$$K(\tau, T(\tau, \kappa)) = \kappa. \tag{5.1}$$

We differentiate this equation with respect to τ and find

$$K_\tau + K_t T_\tau = 0. \tag{5.2}$$

The width of the transition can be discussed as the τ-interval on which κ changes by an increment with order 1; the length of this interval is on the order of the reciprocal of K_τ. During the yielding phase, fast dynamics prevails, which means K_t is of order 1. Hence the width is of the same order as $1/|T_\tau|$.

We review some more useful analysis for $\tau \in [T_{12}^M, T_{12}^e]$ from [44] under imposed constant τ. Regardless of τ, the initial condition is $C_{11} = 1$, $C_{12} = 0$. It is convenient to rewrite the full system in terms of the new variable $u = C_{11} - C_{12}^2$:

$$\begin{aligned} \dot{u} &= \epsilon(C_{12}^2 + u + 3)(C_{12}^2 + 1 - u), \\ \dot{C}_{12} &= \tau - \frac{C_{12}}{C_{12}^2 + u + 3} - \epsilon(C_{12}^2 + u + 3)C_{12}. \end{aligned} \tag{5.3}$$

Fast dynamics means setting $\epsilon = 0$, so that u is constant, and initially $u = 1$. Hence during the initial fast dynamics C_{12} will follow the fast evolution

$$\dot{C}_{12} = \tau - \frac{C_{12}}{C_{12}^2 + 4}. \tag{5.4}$$

If $\tau > 1/4$, the solution of (5.4) grows immediately. The fluid yields in a time of order 1, which is typically thought as "fast". On the other hand, if $\tau < 1/4$, the solution of (5.4) approaches a critical point. At this point, a transition to the slow dynamics occurs. During slow dynamics, the right hand side in the second equation of (5.3) is of order ϵ. That is, approximately, we have

$$u = \frac{C_{12}}{\tau} - C_{12}^2 - 3. \tag{5.5}$$

We can use this relation in the first equation of (5.3) and obtain

$$\big(\frac{1}{\tau} - 2C_{12}\big)\dot{C}_{12} = \epsilon\frac{C_{12}}{\tau}\big(2C_{12}^2 + 4 - \frac{C_{12}}{\tau}\big) \tag{5.6}$$

Slow dynamics breaks down and fast dynamics starts when $C_{12} = 1/(2\tau)$. On the other hand, we reach equilibrium if $2C_{12}^2 + 4 - C_{12}/\tau = 0$.

5.2 Auxiliary dynamic problem

As the above analysis, shear banding occurs at location $y = T_{12}^e$ and later $y = T_{12}^M$ at different moments. The transition mechanism underlying is complex, especially for $y = T_{12}^e$. This

section aims to analyze the dynamics by studying a toy problem related to this case and then clarify the nature of this relationship in the real case later.

When τ is around $T_{12}^e = 1/4$, the flows at $y < T_{12}^e$ transition to slow phase, while verse versa the flows stay in the fast phase. Before discussing the real situation of the local shear band, let's see an initial value ODE problem which could be connected to the original problem. Consider the problem

$$\begin{aligned} \dot{x} &= \epsilon, \\ \dot{y} &= x + y^2, \end{aligned} \tag{5.7}$$

with initial condition $x = x_0$ and $y = y_0$. This dynamics has fast manifold $x = C$ where C is a certain constant and slow manifold $x = -y^2$ (see Figure 5.1).

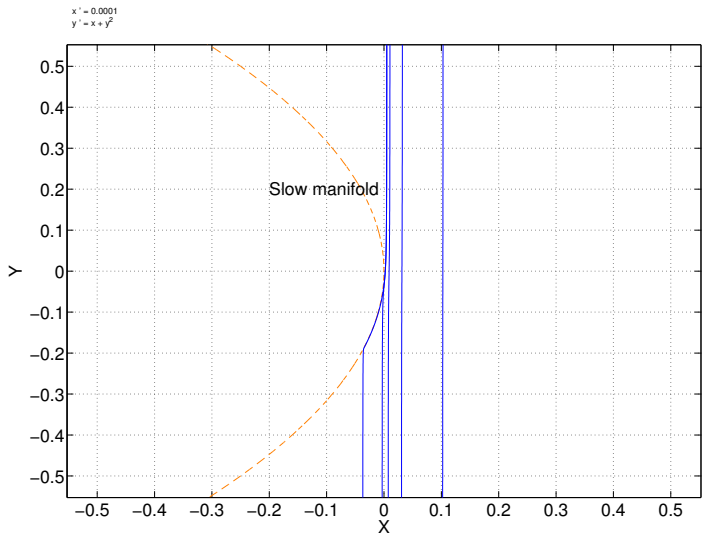

Figure 5.1: Different regimes of flows depend on the distance between initial points $(x_0,\ y_0)$ and slow manifold. The closer the distance is, the more time (larger time scale) the evolution takes.

We shall set $x_0 = \delta$ for a positive δ (different notation from that in last chapter), and y_0 is a negative constant of order 1. We will discuss 3 cases corresponding to 3 different scales of the initial x_0 as follows and later we will see cases corresponding to negative x_0.

1. If $\delta >> \epsilon^{2/3}$, the flow follows the fast regime until y is small of order $\delta^{1/2}$. At this point, the flow gets into a slower phase. Rewrite y's equation as

$$\dot{y} = \delta + y^2. \tag{5.8}$$

If rescaling $y = \sqrt{\delta}\tilde{y}$ and time $t = \delta^{-1/2}\tilde{t}$, the equation changes its form to

$$\frac{d}{d\tilde{t}}\tilde{y} = 1 + \tilde{y}^2 \tag{5.9}$$

with time scale $t \sim \delta^{-1/2}$. Driven by this dynamics, $\tilde{y}$ increases passing 0 to positive numbers with order of $\delta^{-1/2}$. At this time, the flow gets back to the fast regime with $y \sim 1$ and $t \sim 1$. Therefore, the flow spends $O(1)$ time to approach the slow manifold, $\delta^{-1/2}$ time to go through the region near the slow manifold $x = y^2$ and order 1 time evolving to $y = \infty$. In all the flow takes $\delta^{-1/2}$.

2. When $\delta \sim \epsilon^{2/3}$, the ϵ term in x's equation matters when y is sufficiently small. Write y's equation as

$$\dot{y} = \delta + \epsilon t + y^2. \tag{5.10}$$

In fact using $\delta \sim \epsilon^{2/3}$ and the scale analysis of (5.8), $y \sim \epsilon^{1/3}$, $t \sim \epsilon^{-1/3}$, $\epsilon t \sim \epsilon^{2/3}$ which has the same order as δ and y^2. Hence introduce $y = \epsilon^{1/3}$, $t = \epsilon^{-1/3}\tilde{t}$, $\delta = \epsilon^{2/3}\tilde{\delta}$, and we have the rescaling

$$\frac{d}{d\tilde{t}}\tilde{y} = \tilde{\delta} + \tilde{t} + \tilde{y}^2, \tag{5.11}$$

with time scale $t \sim \epsilon^{-1/3}$. Similarly to what happens after the slow phase of the case $\delta >> \epsilon^{2/3}$, the fast dynamics takes over the flow again with a new $x = \delta + M\epsilon^{2/3}$ which is a negative constant of order $\epsilon^{2/3}$. In fast flow, $y \sim 1$ and $t \sim 1$. Hence, the flow takes $\epsilon^{-1/3}$ to increase to $y = \infty$.

3. When $\delta << \epsilon^{2/3}$, we have the similar rescaling as the Case 2. Here $t \sim \epsilon^{-1/3}$, hence $\epsilon t \sim \epsilon^{2/3}$ and δ is negligible. At this moment, if introducing the same rescaling as the Case 2, then

$$\frac{d}{d\tilde{t}}\tilde{y} = \tilde{t} + \tilde{y}^2. \tag{5.12}$$

Analogously to Case 2, x will evolve to $M\epsilon^{2/3}$ and the flow spends $\epsilon^{-1/3}$ time to get $y = \infty$. Therefore, the flow in Case 3 behaves nearly exactly the same as Case 2.

Now consider that $x_0 = -\delta$ and y_0 is still an order 1 negative number. There are basically 3 cases, but the first two of them have already been discussed.

1. This case is for $\delta << \epsilon^{2/3}$. The analysis is the same as the Case 3 when $x_0 = \delta$. The new x value is $M\epsilon^{2/3}$ when the flow gets into fast regime. The time scale of the flow is $\epsilon^{-1/3}$.

2. When $\delta = \epsilon^{2/3}$, the flow takes on the same scales as Case 2 of $x_0 = \delta$ with time scale $\epsilon^{-1/3}$.

3. When $\delta >> \epsilon^{2/3}$, the flow would hit the slow manifold $x = y^2$ and the asymptotic behavior is different from the cases we discussed so far. When the fast curve $x = -\delta$ approaches $x = -y^2$, the flow gets into the slow stage where $x = -\delta + \epsilon t$ with $t \sim \dfrac{\delta}{\epsilon}$ and the y's equation is (5.10) with $y \sim \sqrt{\delta}$. In particular, if $\delta \sim 1$, then $y \sim 1$ and $t \sim \epsilon^{-1}$.

Rescaling $y = \sqrt{\delta}\tilde{y}$, $t = \dfrac{\delta}{\epsilon}\tilde{t}$, we obtain

$$-1 + \tilde{t} + \tilde{y}^2 = 0. \tag{5.13}$$

The derivative term $\dot{y} = \dfrac{\epsilon}{\sqrt{\delta}}\dfrac{d}{d\tilde{t}}\tilde{y} << \epsilon^{2/3}\dfrac{d}{d\tilde{t}}\tilde{y} \sim \epsilon^{2/3}$ is negligible. To the leading order in the original y's equation,

$$-\delta + \epsilon t + y^2 = 0, \tag{5.14}$$

with the solution $y = \sqrt{\delta - \epsilon t}$.

This slow regime breaks down when $\delta \approx \epsilon t$ which means y is small. Let $\epsilon t - \delta = r$, and rescale $r = \epsilon^2\tilde{r}$, $y = \epsilon\tilde{y}$,

$$\frac{d}{d\tilde{r}}\tilde{y} = \tilde{r} + \tilde{y}^2 \tag{5.15}$$

with $t \sim \epsilon^{-1}$. Note the variable r is increasing, hence when $\tilde{r}$ traspasses 0 and behaves like $\epsilon^{-4/3}$, i.e. $x = r \sim \epsilon^{2/3}$, we have a new rescaling $x = \epsilon^{2/3}\tilde{x}$, $y = \epsilon^{1/3}\tilde{y}$ and $t \sim \epsilon^{-1/3}\tilde{t}$. So

$$\frac{d}{d\tilde{t}}\tilde{y} = \tilde{x} + \tilde{y}^2, \tag{5.16}$$

which has same behavior of (5.15). This dynamics breaks down when $y \sim 1$ and the flow gets back to the fast curve $x = M\epsilon^{2/3}$ with positive M and time scale $t \sim 1$ under which the

flow goes to $y = \infty$. Combining these stages, the flow takes $\epsilon^{-1}\delta$ time to evolve from $x = -\delta$ to $x = M\epsilon^{2/3}$, $y = \infty$ on the phase plane.

Combining these discussions, it should be pointed out that there are three different regimes identified other than the fast regime $x = C$: the fast-slow regime (5.8) which is on the fast curve but has a slower time scale, the intermediate stage (5.10) which is a little bit different from the fast curve and has also slower time scale, and slow regime (5.14) which is nearly the slow manifold $x = y^2$. (5.15) and (5.16) are discerned as intermediate regimes.

5.3 Real dynamic problem

In this section, we shall look back to our real problems to find out the scales of time during flow evolution. The clues provided by solving auxiliary problems motivate this following work by using different notations.

When $\tau = 1/4$, the equilibrium point of (5.4) is at $C_{12} = 2$. Now we consider what happens when τ is close to $1/4$, u is close to 1, and C_{12} is close to 2. To analyze the dynamics close to this point, we set $\tau = 1/4 + \sigma$, $v = u - 1$, $c = C_{12} - 2$. Retaining the leading order terms, we have the following expansion for the elastic stress:

$$\frac{C_{12}}{C_{12}^2 + 3 + u} = \frac{1}{4} - \frac{u-1}{32} + \frac{1}{32}(C_{12} - 2)^2. \tag{5.17}$$

Plug this asymptotic regime into (5.3) and using the notations just stipulated, thus the approximated system of (5.3) is obtained:

$$\begin{aligned} \dot{v} &= 32\epsilon, \\ \dot{c} &= \sigma + \frac{v}{32} + \frac{c^2}{32}. \end{aligned} \tag{5.18}$$

Except certain constants of order 1, $\sigma + \frac{v}{32}$ or v is equivalent to x and c is equivalent to y discussed as in the previous section. Therefore, the following discussion is on the track of the auxiliary analysis.

As long as σ is positive and large relative to $\epsilon^{2/3}$, we can set $c = \sqrt{\sigma}\tilde{c}$, $t = \tilde{t}/\sqrt{\sigma}$ and neglect v. Hence the rescaled equation reads

$$\frac{d\tilde{c}}{d\tilde{t}} = 1 + \frac{\tilde{c}^2}{32}. \tag{5.19}$$

The solution of this equation goes from $-\infty$ to ∞ in finite time. Taking into account the rescaling especially, the yield time of order is $1/\sqrt{\sigma}$. If σ is of the same order as $\epsilon^{2/3}$, then the appropriate rescaling of (5.18) is $v = \epsilon^{2/3}\tilde{v}$, $c = \epsilon^{1/3}\tilde{c}$, $\sigma = \epsilon^{2/3}\tilde{\sigma}$, $t = \epsilon^{-1/3}\tilde{t}$. We find a yield time on the order of $\epsilon^{-1/3}$.

Finally, if σ is negative and large relative to $\epsilon^{2/3}$, we must consider that v has to exceed $-\sigma$ before yielding can occur. As long as $\sigma + v/32$ is negative, we may consider the rescaling $v = -\sigma\tilde{v}$, $c = \sqrt{-\sigma}\tilde{c}$, $t = -\sigma/\epsilon\tilde{t}$. This transforms (5.18) into the system

$$\begin{aligned} \frac{d\tilde{v}}{d\tilde{t}} &= 32, \\ \frac{(-\sigma)^{3/2}}{\epsilon}\frac{d\tilde{c}}{d\tilde{t}} &= -1 + \frac{\tilde{v}}{32} + \frac{\tilde{c}^2}{32}. \end{aligned} \tag{5.20}$$

The coefficient of the derivative on the left hand side of the $\tilde{c}$ equation is small, and we neglect this term as long as $\tilde{v} < 32$. However, when $\tilde{v}$ reaches 32, a stationary value of $\tilde{c}$ ceases to exist and starts to grow rapidly. When $\tilde{v}$ comes close to 32, we enter a different regime in which we can rescale (5.18) as follows: $c = \epsilon^{1/3}\tilde{c}$, $v - 32\sigma = \epsilon^{2/3}\tilde{v}$, $t = \epsilon^{-1/3}\tilde{t}$. We then obtain the new system

$$\begin{aligned} \frac{d\tilde{v}}{d\tilde{t}} &= 32, \\ \frac{d\tilde{c}}{d\tilde{t}} &= \frac{\tilde{v}}{32} + \frac{\tilde{c}^2}{32}. \end{aligned} \tag{5.21}$$

This system leads to blowup of $\tilde{c}$ in short time. The dominant contribution to the yield time comes from the slow stage (5.20) and is of order $-\sigma/\epsilon$.

When it comes to the case where $\tau < 1/4$, say, $1/(4\sqrt{2}) < \tau < 1/4$, the yield time is of order $1/\epsilon$ for the existence of the slow manifold. When τ approaches $1/(4\sqrt{2})$, the yield time is lengthened, because the dynamics "almost" reaches an equilibrium on the slow manifold, which stands for completely stopping of the flow. That fixed point is reached when $\tau < 1/(4\sqrt{2})$.

To analyze more closely what comes to the shear banding near $\tau = 1/(4\sqrt{2})$ in long term, we still need to see through the asymptotic regime to find approximate dynamics. We note that at an equilibrium point of (5.3), we have $u = 1 + C_{12}^2$.

As τ is greater than $1/(4\sqrt{2})$, we still can do some substitution for convenience to analyze the asymptotic behavior around the equilibrium. Let $v = u - 1 - C_{12}^2$, then (5.3) takes the form

$$\begin{aligned} \dot{v} + 2C_{12}\dot{C}_{12} &= -\epsilon(2C_{12}^2 + 4 + v)v, \\ \dot{C}_{12} &= \tau - \frac{C_{12}}{2C_{12}^2 + 4 + v} - \epsilon(2C_{12}^2 + 4 + v)C_{12}. \end{aligned} \tag{5.22}$$

Let

$$\phi(C_{12}, v) = \frac{C_{12}}{2C_{12}^2 + 4 + v} + \epsilon(2C_{12}^2 + 4 + v)C_{12}. \tag{5.23}$$

If $\epsilon = 0$, $\phi(C_{12}, 0)$ assumes a maximum at $C_{12} = \sqrt{2}$ and the value of this maximum is $1/4\sqrt{2}$. For nonzero but small ϵ, these numbers get perturbed by $O(\epsilon)$ quantities. We denote these perturbed scalars by c_m and τ_m, i.e.

$$\phi(c_m, 0) = \tau_m, \qquad \frac{\partial \phi}{\partial C_{12}}(c_m, 0) = 0. \tag{5.24}$$

Let perturbation $\sigma = \tau - \tau_m$, $c = C_{12} - c_m$. Noting when for $\epsilon = 0$, we have

$$\frac{\partial \phi}{\partial v}(\sqrt{2}, 0) = -\frac{1}{32\sqrt{2}}, \qquad \frac{\partial^2 \phi}{\partial C_{12}^2}(\sqrt{2}, 0) = -\frac{1}{8\sqrt{2}}, \tag{5.25}$$

which leads to the expansion around $(C_{12},\ v) = (\sqrt{2},\ 0)$ at the leading order:

$$\begin{aligned} \tau - \phi(C_{12}, v) &= \frac{1}{8}[\tau(2C_{12}^2 + v + 4) - C_{12}] \\ &= \tau - \tau_m + \frac{1}{32\sqrt{2}}v + \frac{1}{16\sqrt{2}}(C_{12} - \sqrt{2})^2. \end{aligned} \tag{5.26}$$

Therefore, near $c = 0$, $v = 0$, we have the following leading order terms from (5.22)

$$\begin{aligned} \dot{v} + 2\sqrt{2}\dot{c} &= -8\epsilon v, \\ \dot{c} &= \sigma + \frac{1}{32\sqrt{2}}v + \frac{1}{16\sqrt{2}}c^2. \end{aligned} \tag{5.27}$$

When σ is small, the natural scaling is $c = \sqrt{\sigma}\tilde{c}$, $v = \sigma\tilde{v}$, $t = \tilde{t}/(\epsilon\sqrt{\sigma})$. Hence

$$\begin{aligned} &\delta^{1/2}\frac{d}{d\tilde{t}}\tilde{v} + 2\sqrt{2}\frac{d}{d\tilde{t}}\tilde{c} = -8\tilde{v}, \\ &\epsilon\frac{d}{d\tilde{t}}\tilde{c} = 1 + \frac{1}{32\sqrt{2}}\tilde{v} + \frac{1}{16\sqrt{2}}\tilde{c}^2. \end{aligned} \tag{5.28}$$

This leads to the leading order equation

$$\begin{aligned} 2\sqrt{2}\frac{d\tilde{c}}{d\tilde{t}} &= -8\tilde{v}, \\ 0 &= 1+\frac{1}{32\sqrt{2}}\tilde{v}+\frac{1}{16\sqrt{2}}\tilde{c}^2. \end{aligned} \tag{5.29}$$

We conclude that the yield time behaves as of $\epsilon^{-1}\sigma^{-1/2}$.

Table 5.1 summarizes our results regarding the yield time and the width of the yield zone (i.e. the transition region between low and high shear rate) as a function of τ.

Value of τ	Yield time	Width of yield zone
$\frac{1}{4}+\sigma$, $\sigma >> \epsilon^{2/3}$	$\sigma^{-1/2}$	$\sigma^{3/2}$
$\frac{1}{4}+\sigma$, $\sigma = O(\epsilon^{2/3})$	$\epsilon^{-1/3}$	ϵ
$\frac{1}{4}-\sigma$, $\sigma >> \epsilon^{2/3}$	$\sigma\epsilon^{-1}$	ϵ
between $1/(4\sqrt{2})$ and $1/4$	ϵ^{-1}	ϵ
$\tau_m+\sigma$, $\sigma > 0$	$\epsilon^{-1}\sigma^{-1/2}$	$\epsilon\sigma^{3/2}$

Table 5.1: Yield time and width of yield zone as a function of shear stress.

Viscometric devices, for instance in [56], in contrast to Poiseuille flow, are aimed for a uniform shear stress across the flow domain. However, due to experimental imperfections, small variations in shear stress may raise some problems. If the shear stress is in the range where delayed yielding occurs, then the variation in shear stresses translates into a difference among yield time, and since the yield time is large (of order $1/\epsilon$), this variation in yield time may be amplified to be noticeable even if the difference in shear stress is small. The consequence is transient shear banding, i.e. shear bands develop temporarily even though eventually there is uniform yielding across the entire gap. Such a case is studied in [37] for a model which is different from ours but shares some of the qualitative features; we note that their Figure 5.2 clearly shows delayed yielding.

We shall display some numerical results illustrating the asymptotic findings of Table 5.1. The first part of Figure 5.2 shows the yield location as a function of time. The value of ϵ is 10^{-4}. To find the yield location, we solve the system of (1.5) and (1.6) for τ in the range $[0.17, 0.28]$. This yields the shear rate as a function of τ and time. During yielding, the shear rate goes from a value close to 0 to a value close to τ in a short interval of time. We have arbitrarily picked the intermediate value $\kappa = 0.1$ as the "yield location". That is, Figure 5.2 shows the value of τ at which $\kappa = 0.1$ as a function of time. At short times, the yield location is close to $\tau = 1/4$, while at long time it approaches $\tau = \tau_m \sim 1/(4\sqrt{2})$. According to Table 5.1, $\tau - 1/4$ at short times, and $\tau - \tau_m$ at long times should both be proportional to t^{-2} ($\tau - 1/4$ and $\tau - \tau_m$, resp., are proportional to δ and the yield time is proportional to $\delta^{-1/2}$). The slope of the log-log plots in the second and third parts of Figure 1 is consistent with this. We used $\epsilon = 0$ for the second plot of Figure 5.3, while for the third plot we have $\epsilon = 10^{-4}$ as in part 1 of the figure. We note that for the asymptotics in the first row of Table

5.1, we need $1 << t << \epsilon^{-1/3}$. It is difficult to observe this asymptotic regime "cleanly" unless ϵ is very small. The fourth part of Figure 5.2 illustrates this for $\epsilon = 10^{-5}$. The slope in the log-log plot initially approaches 2, but the condition that t must be small relative to $\epsilon^{-1/3}$ becomes violated before the asymptotic regime can become clearly established.

The first two plots of Figure 5.2 show the shear rate as a function of τ at two different times. As expected, the yield location moves to the left and the transition sharpens as time is increased. To compare with the asymptotics of Table 5.1, we need a working definition of "width". For this purpose, we look at derivatives of the shear rate κ with respect to τ, which we calculate numerically by finite differences. The third and fourth subplot of Figure 5.3 show the first and second derivatives. We use the distance between the maximum and minimum of the second derivative as a convenient measure for the width of the transition zone. In Figure 5.4, we plot the width of the transition zone determined in this fashion. Table 5.1 predicts a behavior like t^{-3} for times short relative to $\epsilon^{-1/3}$ as well as for times long relative to ϵ^{-1}. The slopes of the log-log plots are close to -3 illustrating this behavior. As in Figure 5.4, we have used $\epsilon = 0$ for the short time plot such as the flow stays in fast dynamics for capturing ease, and $\epsilon = 10^{-4}$ for the long time plot.

5.4 Shear banding with Korteweg stress

In the context of the Larson's PEC model, we have proposed a theory to estimate where the location of shear transition is. But it is not the real picture of shear banding. In this section, we will address this issue by utilizing Korteweg stress effect on the PEC model. We have interpreted $\mathbf{C}$ as tube conformation tensor, and there is interfacial energy is associated with a tube conformation mismatch. The effect of Korteweg stresses is added into the momentum balance equation (1.6), which now turns out to be

$$T_{12} + \eta\kappa + T_K = \tau, \tag{5.30}$$

with T_K denoting the Korteweg stress.

We shall consider two different expressions for the interfacial energy and associated Korteweg stresses. In Model 1, the interfacial energy density is given by

$$W = \delta^2 (C'_{11})^2, \tag{5.31}$$

and the coresponding Korteweg stress is as indicated by the relation deducted in [45]

$$T_K = -4\delta^2 C_{12} C''_{11}. \tag{5.32}$$

Here a prime denotes the derivative with respect to y. The parameter δ we reuse is a small constant associated with the Korteweg stress; this parameter has nothing to do with δ used

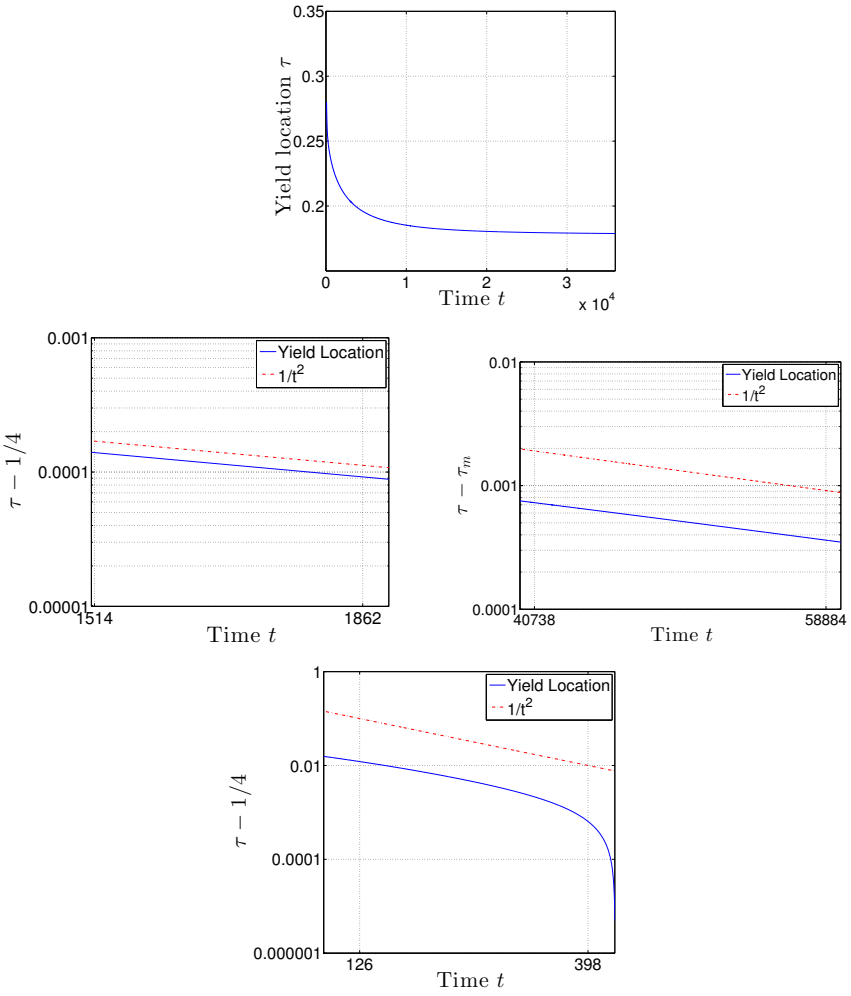

Figure 5.2: The first plot shows the yield location as a function of time for $\epsilon = 10^{-4}$. As predicted by the asymptotics, the yield location approaches 0.25 for short time and then converges to $\tau_m \sim 1/(4\sqrt{2})$ on a time scale of order $1/\epsilon$. The second and third part of the plot show the t^{-2} behavior of $\tau - 1/4$ and $\tau - \tau_m$, respectively. The value of ϵ is zero for the second plot and 10^{-4} for the third plot. The fourth plot shows $\tau - 1/4$ for $\epsilon = 10^{-5}$. Note that the asymptotics predicts a slope of -2 only for $1 << t << \epsilon^{-1/3}$.

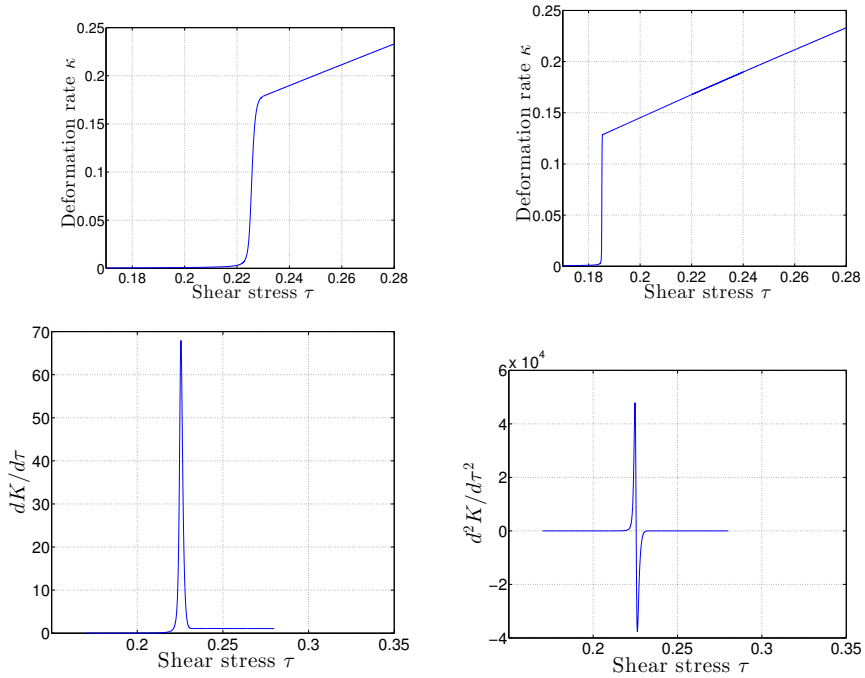

Figure 5.3: The first two subfigures show the shear rate at two different fixed times. The sharp transition shifts to smaller values of τ as time increases.The third and fourth subfigures show the derivatives of the shear rate with respect to τ corresponding to the data of the first subplot. The value of ϵ is 10^{-4}.

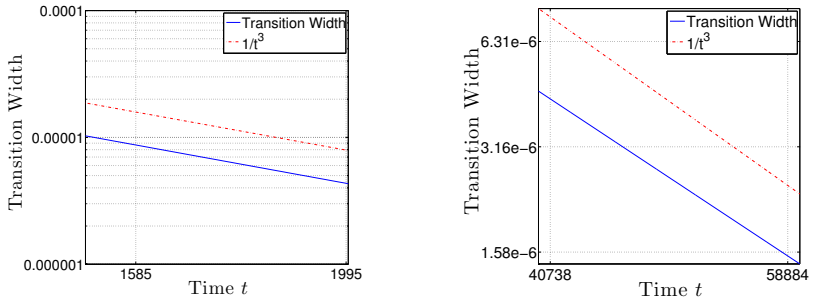

Figure 5.4: When $\epsilon = 0$, the transition zone approaches $\tau = 1/4$. The width of the transition behaves like t^{-3} as illustrated in the first plot. If ϵ is nonzero, and time is large relative to $1/\epsilon$, the transition zone approaches $\tau = \tau_m$, with the width also behaving like t^{-3}. The second plot shows this behavior for $\epsilon = 10^{-4}$.

in section 4.4, and Table 5.1. This expression for W is mathematically simple, but we note that C_{11} is much larger in the yielded phase than in the unyielded phase for high scale deformation. Therefore this model predicts rather asymmetric Korteweg stressses during a short time. To reduce this asymmetry, we modify the energy density for our Model 2:

$$W = \delta^2 (C_{11}')^2 / C_{11}. \tag{5.33}$$

The corresponding Korteweg stress is

$$T_K = -4\delta^2 \frac{C_{12}}{C_{11}} C_{11}'' + 2\delta^2 \frac{C_{12}}{C_{11}^2} (C_{11}')^2. \tag{5.34}$$

The Korteweg stress has two effects: First, it moderates the transition between yielded and unyielded regions. If δ is small, then the results will initially be similar to those for $\delta = 0$, but after a long time the sharpening of the transition will stop, and there will be a finite width of order δ. Another, more important and complex effect is that the location of the transition will change during evolution. Without regularizing effect, we found that the eventual position of the shear banding transition is always at $\tau_m = 1/(4\sqrt{2}) + O(\epsilon)$. With Korteweg stresses, we shall observe this for shorter times, but eventually the location of the transition is modified to a new equilibrium location determined by an admissibility principle: the equal area rule as derived in [45]. The precise form of this equal area rule should depend on the form of the Korteweg stress. However, for any interfacial energy density of the form $W = a(C_{11})(C_{11}')^2$, and therefore the both models above, it satisfies the form

$$\int \Big[g(C_{12}) - \tau \Big] \, dC_{12} = 0, \tag{5.35}$$

where

$$g(C_{12}) = \frac{C_{12}}{2C_{12}^2 + 4} + \epsilon(2C_{12}^2 + 4)C_{12}, \tag{5.36}$$

is the shear stress in steady state, and the lower and upper limits of the integral are the values of C_{12} on both sides of the deformation transition, i.e. the integration is over the C_{12} region from the smallest to the largest root of the equation $g(C_{12}) = \tau$. As $\epsilon = 10^{-5}$, clarified in the computations, the numerical value of the band location obtained from this rule is approximately $\tau = 0.09731$.

For these computations, we used $\epsilon = 10^{-5}$, $\delta = 10^{-6}$. Figure 5.5 shows a comparison of the shear banding transition with and without Korteweg stresses in Model 1. The three plots show the components C_{11} and C_{12} of the conformation tensor and the shear rate κ across the transition zone. At the time where this is plotted ($t = 10000$ which stands for long time), the location of the transition with and without Korteweg stresses has begun

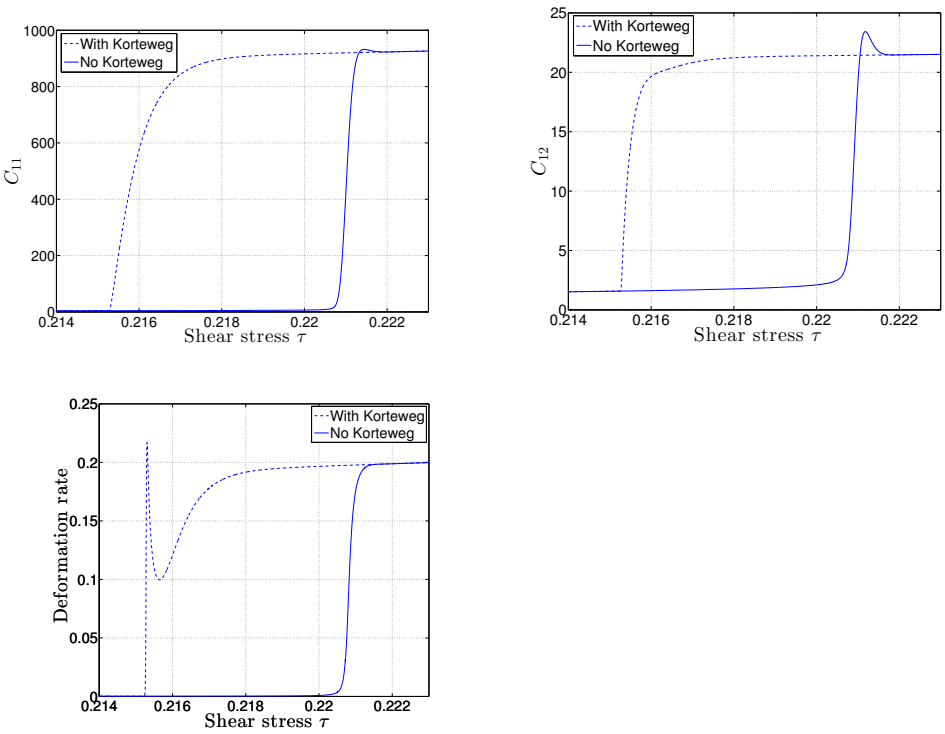

Figure 5.5: Comparison of shear banding transitions with and without Korteweg stresses, Model 1, at $t = 10000$.

to differ apparently. As expected, the Korteweg stresses also expand the transition zone. We also observe a nonmonotonicity of the shear rate across the transition whereas such nonmonotonicity is observed for the components of the conformation tensor. Figure 5.6 shows the corresponding computation for Model 2. For this model, the interfacial energy is different by a factor $1/C_{11}$ eliminating its scale, and since C_{11} becomes large (of order $\epsilon^{-2/3}$) during yielding, the overall Korteweg stress is smaller than Model 1. It hence takes longer before Korteweg stresses have a noticeable effect, and the plots are at time as longer as $t = 70000$ rather than 10000. Since the Korteweg stress is smaller, we also have less smoothing of the transition zone. The nonmonotonicity of shear rate which was observed with Model 1 does not appear as W has been scaled down.

Figure 5.7 shows a plot of the shear rate in the final equilibrium reached for both models. The position of the transition zone is in excellent consistency with our prediction of $\tau = 0.09731$. The width of the transition is greater for Model 1. The nonmonotonicity of shear rate, which was observed for earlier times, no longer appears eventually.

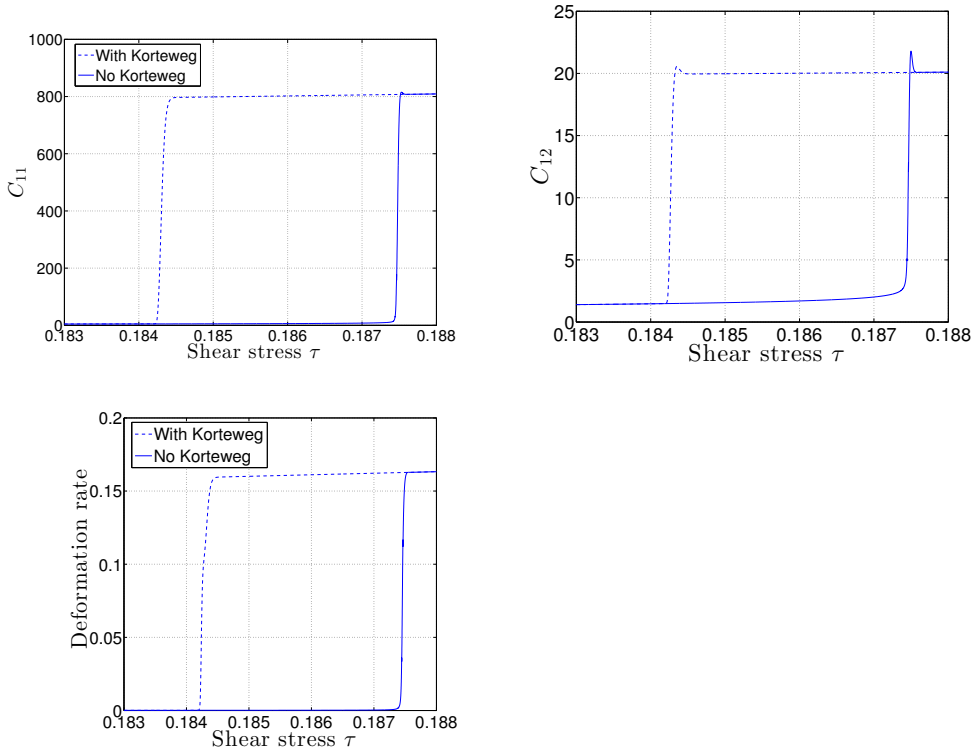

Figure 5.6: Comparison of shear banding transitions with and without Korteweg stresses, Model 2, at $t = 70000$.

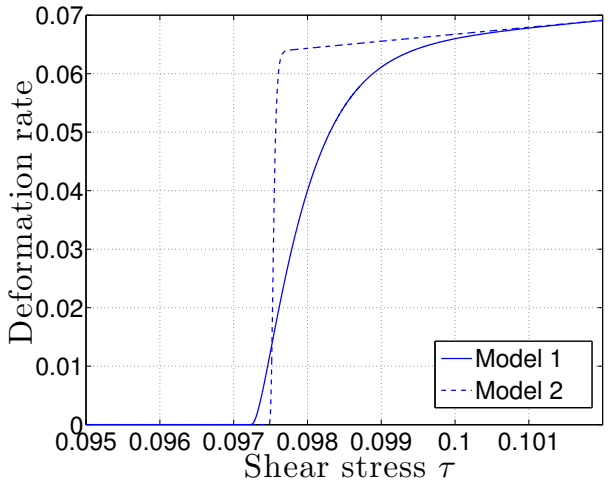

Figure 5.7: Final position of shear banding transition for Model 1 ($t = 9,620,000$) and Model 2 ($t = 33,850,000$).

Conclusion

We have analyzed problems from shear flow of thixotropic fluids. In this dissertation, the oscillatory stress experiment is analyzed and simulated in theoretic aspect. We try to simplify the setting compared to real fluid experiments and have studied many parameter regimes to investigate the essential mechanisms of thixotropic behaviors. Furthermore, the steady shear flows producing spatial inhomogeneity are also inspected to study the shear bands. The equal area rule is included in to predict band location in real situations.

The following problems remain potential future study:

- We have done analysis on the case where we control the total stress to be a sinusoidal input, however leave prescribing strain experiments open. In fact, these strain-controlled experiments are done more these days in laboratory or simulations. However, theoretic results are fewer to compare or predict their results.
- The shear bands are not analyzed in oscillatory Poiseuille flow. The oscillation shears and destroys the microstructure within many cycles and definitely it will impact to shape shear bands. The future theoretic efforts could address this.

Acknowledgement

At the end of this dissertation, the author, Taige Wang, appreciates his advisor Professor Michael Renardy for his precious advice on thinking, formulating, and analyzing problems and indispensable support from him. The author really learns a lot from his conscientious attitude and creative insight. The author also wants to thank all the defense committee members: Professor Yuriko Renardy, Professor Robert Rogers and Professor Shu-Ming Sun for their professional guidance. The author wants to thank GTA mentors and coordinators: Eileen Shugart, Dr. Nicholas Robbins, Dr. Rachel Arnold, Nichole Sutphin, technician Ken Hinson and Bill Reilly, and Department of Mathematics for their constant help, sincere guidance, and support on research and work during these 5 years. As well, the author wants to show gratitude to Professor John Burns and Professor Donald Baird for their enthusiastic help and knowledgable instructions, to Professor Zhuangyi Liu from University of Minnesota, Professor Xiaoming Wang from Florida State University, and M.S. advisor Professor Yuming Qin, B.S. advisor Professor Feng Xie from Donghua University and other professors who ever taught the author classes for their encouragement, support, and suggestions these years. Without their warmhearted care, informative discussions and valuable suggestions impacting on author's work and life, he can't go this further.

The author takes this opportunity to thank senior and current peers who impact author's research and life all the time: Dr. Xiaojun Wang, Dr. Xu Zhang, Dr. Boris Kramer, Mr. Kihyo Moon, Mrs. Holly V. Grant, Dr. Yu Ran, Dr. Zhu Wang, Dr. Weiwei Hu from our Math department, graduate fellow students Mr. Peng Zhang from Department of Engineering Science and Mechanics, Mr. Rui Sun and Mr. Jianxun Wang from Department of Aerospace and Ocean Engineering, Dr. Yukun Li from University of Tennessee, other fellow graduate students and dear friends for their inspiring discussions and enjoyable time spent with the author.

Last but not least, Taige Wang, wants to express his thanks to his parents Weiming Wang and Xiangli Jia, Grandmother Peiying Gao, Uncle Zhedong Wang, Aunt Yu Wang, Ping Wang, and other relatives for their great love, help, support and advice.

Bibliography

[1] R. Abeyaratne and J.K. Knowles, *Evolution of Phase Transitions: A Continuum Theory*, Cambridge 2006.

[2] E.C. Aifantis and J.B. Serrin, The mechanical theory of fluid interfaces and Maxwell's Rule, *J. Coll. Interface Sci.* **96** (1983) 517-529.

[3] V.J. Anderson, J.R.A. Pearson and E.S. Boek, The rheology of worm-like micellar fluids, *Rheology Reviews* 2006, 217-254.

[4] H.A. Barnes and K. Walters, The yield stress myth?, *Rheol. Acta* **24** (1985), 323-326.

[5] H.A. Barnes, Review Thixotropy–a review, *J. Non-Newt. Fluid Mech.* **70** (1997), 1-33.

[6] H.A. Barnes, The yield stress – a review, or '$\pi\alpha\nu\tau\alpha\ \rho\epsilon\iota$' – everything flows, *J. Non-Newt. Fluid Mech.* **81** (1999), 133-178.

[7] R.B. Bird, R.C. Armstrong and O. Hassager, Dynamics of polymeric liquids: Fluid mechanics, 2nd Edition, John Wiley & Sons, 1987.

[8] H.C. Blackwell and R.H. Ewoldt, A simple thixotropic-viscoelastic constitutive model produces unique signatures in large-amplitude oscillatory shear (LAOS), *J. Non-Newt. Fluid Mech.* **208-209** (2014), 27-41.

[9] J.W. Cahn and J.E. Hilliard, Free energy of a nonuniform system. I. Interfacial free energy, *J. Chem. Phys.* **28** (1958), 258-267.

[10] M.E. Cates and S.M. Fielding, Rheology of giant micelles, *Adv. Phys.* **55** (2006), 799-879.

[11] F. Caton and C. Baravian, Plastic behavior of some yield stress fluids: from creep to long-time yield, *Rheol. Acta* **47** (2008), 601-607.

[12] D.C.-H. Cheng, Yield stress: A time dependent property and how to measure it, *Rheol. Acta* **25** (1986), 542-554.

[13] K.S. Cho, K. Hyun, K.H. Ahn and S. J. Lee, An geometric interpretation of large amplitude oscillatory shear response, *J. Rheo.* **49(3)** (2005), 747-758.

[14] P. Coussot and F. Gaulard, Gravity flow instability of viscoplastic materials: The ketchup drip, *Phys. Rev. E* **72** (2005), 031409.

[15] M. Cromer, L.P. Cook and G.H. McKinley, Extensional flow of wormlike micellar solutions, *Chem. Eng. Sci.* **64** (2009), 4588-4596.

[16] C. Dimitriou, L. Casanellas, T.J. Ober and G.H. McKinley, Rheo-PIV of a shear-banding wormlike micellar solution under large amplitude oscillatory shear, Rheol. Acta **51** (2012), 395-411.

[17] C. Dimitriou, R. Ewoldt and G. McKinley, Describing and prescribing the constitutive response of yield stress fluids using large amplitude oscillatory shear stress (LAOStress), *J. Rheol.* **57** (2013), 27-70.

[18] A. Dorfmann and R.W. Ogden, A constitutive model for the Mullins effect with permanent set in particle-reinforced rubber, *Int. J. Solids Struct.* **41** (2004), 1855-1878.

[19] J.E. Dunn and J. Serrin, On the thermomechanics of interstitial working, *Arch. Rational Mech. Anal.* **88** (1985), 95-133.

[20] J.L. Ericksen, Equilibrium of bars, *J. Elasticity* **5** (1975), 191-201.

[21] M.A. Fardin et al., Potential "ways of thinking" about the shear-banding phenomenon, *Soft Matter* **8** (2012), 910-922.

[22] S.M. Fielding, Shear banding, aging and noise dynamics in soft, glassy materials, *Soft Matter* **5** (2009), 2378-2382.

[23] H. Frunlich, Thixotropie, Hermann, Paris, 1935.

[24] E. Fried and M.E. Gurtin, Dynamic solid-solid transitions with phase characterized by an order parameter, *Physica D* **72** (1994), 287-308.

[25] E. Fried and G. Grach, An order-parameter based theory as a regularization of a sharp-interface theory for solid-solid phase transitions, *Arch. Rational Mech. Anal.* **138** (1997), 355-404.

[26] R. Grimshaw, *Nonlinear Ordinary Differential Equations*, CRC Press, Boca Raton 1993.

[27] A.E. James, D.J.A. Williams and P.R. Williams, Direct measurement of static yield properties of cohesive suspensions, *Rheol. Acta* **26** (1987), 437-446.

[28] D.J. Korteweg, Sur la forme que prennent les équations du mouvements des fluides si l'on tient compte des forces capillaires causées par des variations de densité considérables mais continués et sur la theorie de la capillarité dans l'hypothèse d'une variation continué de la densité, *Arch. Need. Sci. Exactes Nat. Ser. II* **6** (1901) 1-24.

[29] R.G. Larson, A constitutive equation for polymer melts based on partially extending strand convection, *J. Rheol.* **28** (1984), 545-571.

[30] R.G. Larson, Constitutive equations for polymer melts and solutions, Butterworths, Boston, 1988.

[31] C.-Y.D. Lu, P.D. Olmsted and R.C. Ball, Effects of non-local stress on the determination of shear banding flow, *Phys. Rev. Lett.* **84** (2000), 642-645.

[32] K.L. Maki and Y. Renardy, The dynamics of a viscoelastic fluid which displays thixotopic yield stress behavior, *J. Non-Newt. Fluid Mech.* **181-182** (2012), 30-50.

[33] L. Martinie, H. Buggisch and N. Willenbacher, Apparent elongational yield stress of soft matter, *J. Rheol.* **57** (2013), 627-646.

[34] J. Mewis and N.J. Wagner, Thixotropy, *Advances in Colloid and Interface Science* **147-148** (2009), 214-227.

[35] R.D. Mindlin, Second gradient of strain and surface tension in linear elasticity, *lnt. J. Solids Struct.* **1** (1965), 417-438.

[36] P.C.F. Møller, J. Mewis and D. Bonn, Yield stress and thixotropy: on the difficulty of measuring yield stresses in practice, *Soft Matter* **2** (2006), 274-283.

[37] R.L. Moorcroft and S.M. Fielding, Criteria for shear banding in time-dependent flows of complex fluids, *Phys. Rev. Lett.* **110** (2013), 086001.

[38] Q.D. Nguyen and D.V. Boger, Measuring the flow properties of yield stress fluids, *Ann. Rev. Fluid Mech.* **24** (1992), 57-88.

[39] G. Picard, A. Ajdari, L. Bocquet and F. Lecqueux, Simple model for heterogeneous flows of yield stress fluids, *Phys. Rev. E* **66** (2002), 051501, 1-12.

[40] T. Peterfi, Arch. Entwicklungsmesh. Organ **112** (1927) 680, Verhandlungen 3rd. Intern Zellforschung-Kongr., Arch. Exp. Zellf, **15** (1934), 373.

[41] J. Paredes, N. Shahidzadeh-Bonn and D. Bonn, Shear banding in thixotropic and normal emulsions, *J. Phys. Condensed Matter* **23** (2011), 284116.

[42] J. Pryce-Jones, JOCCA, **17** (1934) 305; **19** (1936), 395; **26** (1943), 3.

[43] M. Renardy, Mathematical Analysis of Viscoelastic Flows, CBMS-NSF Conference Series in Applied Mathematics 73, SIAM 2000, 104 pp.

[44] M. Renardy, The mathematics of myth: Yield stress behavior as a limit of nonmonotone constitutive theories, *J. Non-Newt. Fluid Mech.* **165** (2010), 519-526.

[45] M. Renardy, Korteweg stresses and admissibility criteria for shear banded flows, *J. Non-Newt. Fluid Mech.* **213** (2014), 68-72.

[46] M. Renardy and T. Wang, Large amplitude oscillatory shear flows for a model of a thixotropic yield stress fluid, *J. Non-Newt. Fluid Mech.* **222** (2015), 1-17.

[47] M. Renardy and T. Wang, Development of shear bands for a model of a thixotropic yield stress fluid, *J. Non-Newt. Fluid Mech.*, to appear.

[48] Y. Renardy and H.V. Grant, Uniaxial extensional flow of a thixotropic yield stress fluid: a viscoelastic model, *Rheol. Acta* **52** (2013), 867-879.

[49] N.E. Spenley, X.F. Yuan and M.E. Cates, Nonmonotonic constitutive laws and the formation of shear-banded flows, J. Physique II **6** (1996), 551-571.

[50] J.R. Stokes and J.H. Telford, Measuring the yield behaviour of structured fluids, *J. Non-Newt. Fluid Mech.* **124** (2004), 137-146.

[51] N. Triantafyllidis and E.C. Aifantis, A gradient approach to localization of deformation. I. Hyperelastic materials, *J. Elasticity* **16** (1986), 225-237.

[52] J.D. van der Waals, Theorie thermodynamique de la capillarité dans l'hypothèse d'une variation continué de densité, *Arch. Neerl. Sci. Exactes Nat.* **28** (1895), 121-209.

[53] C.C. White and D.L. Hunston, Characterizing the nonlinear viscoelastic properties of sealant, including its Mullins effect, *Polymer Eng. Sci.* **48** (2008), 2317-2328.

[54] P.A. Vasquez, G.H. McKinley and L.P. Cook, A network scission model for wormlinke micellar solutions I. Model formulation and viscometric flow predictions, *J. Non-Newt. Fluid Mech.* **144** (2007), 122-139.

[55] L. Zhou, P.A. Vasquez, L.P. Cook and G.H. McKinley, Modeling the inhomogeneous response and formation of shear bands in steady and transient flows of entangled liquids, *J. Rheol.* **52** (2008), 591-623.

[56] L. Zhou, L.P. Cook and G.H. McKinley, Probing shear-banding transitions of the VCM model for entangled wormlike micellar solutions using large amplitude oscillatory shear (LAOS) deformations, *J. Non-Newt. Fluid Mech.* **165** (2010), 1462-1472.